Polyakov SU(3) extended linear-σ model: Sixteen mesonic states in chiral phase structure

Abdel Nasser Tawfik*
Egyptian Center for Theoretical Physics (ECTP), Modern University for Technology and Information (MTI), 11571 Cairo, Egypt and World Laboratory for Cosmology And Particle Physics (WLCAPP), Cairo, Egypt

Abdel Magied Diab
World Laboratory for Cosmology And Particle Physics (WLCAPP), Cairo, Egypt

(Received 23 May 2014; revised manuscript received 23 October 2014; published 16 January 2015)

In the mean field approximation, the derivative of the grand potential, nonstrange and strange condensates, and the deconfinement phase transition in a thermal and dense hadronic medium are verified in the SU(3) Polyakov linear-σ model (PLSM). The chiral condensates σ_x and σ_y are analyzed with the goal of determining the chiral phase transition. The temperature and density dependences of the chiral mesonic phase structures are taken as free parameters and fitted experimentally. They are classified according to the scalar meson nonets: (pseudo)scalar and (axial) vector. For the deconfinement phase transition, the effective Polyakov-loop potentials ϕ and ϕ^* are implemented. The in-medium effects on the masses of sixteen mesonic states are investigated. The results are presented for two different forms for the effective Polyakov-loop potential and compared with other models, which include and exclude the anomalous terms. It is found that the Polyakov-loop potential has considerable effects on the chiral phase transition so that the restoration of the chiral symmetry breaking becomes sharper and faster. Assuming that the Matsubara frequencies contribute to the meson masses, we have normalized all mesonic states with respect to the lowest frequency. By doing this, we characterize temperatures and chemical potentials at which the different meson states dissolve to *free* quarks. Different dissolving temperatures and chemical potentials are estimated. The different meson states survive the *typically averaged* QCD phase boundary, which is defined by the QCD critical temperatures at varying chemical potentials. The thermal behavior of all meson masses has been investigated in the large-N_c limit. It is found that, at high T, the scalar meson masses are T independent (except π and σ). For the pseudoscalar meson masses, the large-N_c limit unifies the T dependences of the various states into a universal bundle. The same is also observed for axial and axial-vector meson masses.

DOI: 10.1103/PhysRevC.91.015204 PACS number(s): 12.39.Fe, 12.40.Yx, 14.40.−n

I. INTRODUCTION

The systematic study of strongly interacting matter at finite density allows analysis of special theories that probably agree with the heavy-ion experiments aiming to tackle the quantum chromodynamic (QCD) phase-transition between combined nuclear matter and the quark-gluon plasma (QGP) and to improve our understanding of the evolution of the early Universe. All these can be probed in experiments such as STAR at the Relativistic Heavy Ion Collider (RHIC, at BNL), ALICE at the Large Hadron Collider (LHC, at CERN), Compressed Baryon Matter (CBM) at the Facility for Antiproton and Ion Reaserch (GSI), and Baryonic Matter at the Nuclotron (BM@N) at the Nuclotron-Based Ion Collider Facility (JINR). In-medium effects on thermodynamics quantities are presented in the numerical solutions of difference effective models, especially the QCD-like ones. There are two main first-principle models: the Polyakov Nambu-Jona-Lasinio (PNJL) and Polyakov linear-σ model (PLSM) or the Polyakov quark meson (PQM) model.

As the finite quark masses break the chiral symmetry of QCD explicitly, one has to resort to numerical calculations in order to determine the chiral phase transition, such as the $SU(3)_r \times SU(3)_\ell$ linear-σ model [1]. Thus, $SU(3)_l \times SU(3)_r \times U(1)_A \rightarrow SU(3)_V \times SU(3)_A$. A long time ago, the quark constituents of scalar mesons were debated [2,3]. Accordingly, the determination of all meson states is possible: $\langle \bar{q}q \rangle = \langle \bar{q}_r q_\ell + \bar{q}_\ell q_r \rangle \neq 0$ [4]. The chiral structure of the four categories of the meson states is classified through quantum numbers, orbital angular momentum J, parity P, and charge conjugate C, which can be constructed from u and d, and s quarks, into scalars ($J^{PC} = 0^{++}$) and pseudoscalars ($J^{PC} = 0^{-+}$), vectors ($J^{PC} = 1^{-}$) and axial vectors ($J^{PC} = 1^{++}$). As the chiral symmetry is explicitly broken, the deconfinement phase transition likely affects the mass spectrum and shows under which conditions certain states degenerate with another one and when the thermal and density evolution goes through a phase transition.

In the present work, the in-medium effects on the masses of different meson states are analyzed systematically. We study the effects of finite temperature on sixteen meson states at vanishing and finite baryon-chemical potentials and also their density dependence at finite temperatures. To this end, extending LSM to PLSM, in which information about the confining gluonic sector is also embedded in the form of the Polyakov-loop potential, is very crucial. The Polyakov-loop potential is extracted from pure Yang-Mills lattice simulations [5–8]. In investigating the chiral phase transition, LSM at finite temperature has been implemented [9,10]. Furthermore, $U(N_f)_r \times U(N_f)_l$ LSM with $N_f = 2, 3$, or even 4 quark flavors has been analyzed [11–14].

*http://atawfik.net/

LSM thermodynamic properties such as pressure, equation of state, speed of sound, specific heat, and trace anomaly can be evaluated at finite and vanishing baryon chemical potential [15–19] and under effects of an external magmatic field [20]. Furthermore, the normalized and non-normalized higher-order moments of the particle multiplicity are investigated [18,21,22]. With the inclusion of the Polyakov-loop correction, the chiral phase structure of the scalar and pseudoscalar meson states at finite and vanishing temperatures has been evaluated [23] with and without axial anomaly [24,25]. At finite isospin chemical potential, a three-flavor NJL model for scalar and pseudoscalar mesonic states was presented in Ref. [26]. In the three-flavor PNJL model [27], it is found that the inclusion of the Polyakov-loop potential in the NJL model considerably affects the meson masses. Results from $2+1$ lattice QCD for pseudoscalar and vector meson states [28–31] and QCD thermodynamics including meson masses at vanishing temperature have been reported [32]. The results deduced from the HotQCD [30] and PACS-CS [31] Collaborations are compared with the Particle Data Group (PDG) [33]. An excellent agreement was presented in Refs. [23–26,30,31,33].

In general, PLSM has a wide range of implications. It can describe not only the thermodynamics [16,18,34,35] but also the higher-order moments of the particle multiplicity [18,21], the hadron vacuum phenomenology [36–40], and the effects of the chiral and deconfinement phase transitions [41–43] besides the chiral phase structure of hadrons (the spectrum of hadrons in both thermal and hadronic dense medium) [23–25,44,45], and the decay width and the scattering length of hadronic states [36–38,40,46,47].

In the present work, we introduce a systematic study using the chiral symmetric linear-σ model. We included in it scalar, pseudoscalar, vector, and axial-vector fields and estimate the representation of all these four categories in dependence on the temperature T and the baryon chemical potential μ. This allows us to define the characteristics of the chiral phase structure for all these meson states in thermal and dense medium and determine the critical temperature and density at which each meson state breaks into its free quarks.

The present paper is organized as follows. Section II gives details about the SU(3) Polyakov linear-σ model (PLSM), where the Lagrangians of the scalar and pseudoscalar fields are extended to include vector and axial-vector fields as well and interaction between mesonic sectors in the presence of $U(1)_A$ symmetry breaking. The Polyakov-loop correction to the Lagrangian of PLSM is introduced in Sec. II A. The mean field approximation is outlined in Sec. II B. The phase transition including quark condensates and order parameters is estimated in Sec. III. Topics such as deconfinement (crossover) phase transition and order parameter due to chiral symmetry breaking are studied as well. In Sec. IV, we introduce the Polyakov-loop potential to LSM and investigate sixteen mesonic states in thermal (Sec. IV A 1) and hadronic dense medium (Sec. IV A 2). The critical temperature and the baryon chemical potential, at which each bound hadron state should dissolve into free quarks (QGP)is introduced in Sec. V. Section VII is devoted to the conclusions.

II. SU(3) POLYAKOV LINEAR-σ MODEL

The Lagrangian of LSM with $N_f = 3$ quark flavors and $N_c = 3$ color degrees of freedom, where the quarks couple to the Polyakov-loop dynamics Φ field, represents a complex (3×3) matrix for the $SU(3)_L\times SU(3)_R$ symmetric LSM Lagrangian $\mathcal{L}_{\rm chiral} = \mathcal{L}_q + \mathcal{L}_m$, where the fermionic part reads

$$\mathcal{L}_q = \bar{q}\left[i\partial\!\!\!/ - g\ T_a\left(\sigma_a + i\,\gamma_5\,\pi_a + \gamma_\mu V_a^\mu + \gamma_\mu\gamma_5 A_a^\mu\right)\right]q, \quad (1)$$

where μ is an additional Lorentz index [48] and g is the flavor-blind Yukawa coupling of the quarks to the mesonic contribution $\mathcal{L}_m = \mathcal{L}_{SP} + \mathcal{L}_{VA} + \mathcal{L}_{\rm Int} + \mathcal{L}_{U(1)_A}$, with $\mathcal{L}_{SP}$ representing scalars ($J^{PC} = 0^{++}$) and pseudoscalars ($J^{PC} = 0^{-+}$), $\mathcal{L}_{VA}$ representing vector ($J^{PC} = 1^{-01}$) and axial-vector ($J^{PC} = 1^{++}$) mesons, and $\mathcal{L}_{\rm Int}$ being the interaction between them. Finally the Lagrangian of the anomaly term is given by $\mathcal{L}_{U(1)_A}$ [1,47,49–52]:

$$\begin{aligned}\mathcal{L}_{SP} &= {\rm Tr}(\partial_\mu\Phi^\dagger\partial^\mu\Phi - m^2\Phi^\dagger\Phi) - \lambda_1[{\rm Tr}(\Phi^\dagger\Phi)]^2 \\ &\quad - \lambda_2{\rm Tr}(\Phi^\dagger\Phi)^2 + {\rm Tr}[H(\Phi+\Phi^\dagger)], \quad (2)\\ \mathcal{L}_{AV} &= -\frac{1}{4}{\rm Tr}\left(L_{\mu\nu}^2 + R_{\mu\nu}^2\right) + {\rm Tr}\left[\left(\frac{m_1^2}{2}+\Delta\right)\left(L_\mu^2+R_\mu^2\right)\right] \\ &\quad + i\frac{g_2}{2}({\rm Tr}\{L_{\mu\nu}[L^\mu,L^\nu]\} + {\rm Tr}\{R_{\mu\nu}[R^\mu,R^\nu]\}) \\ &\quad + g_3[{\rm Tr}(L_\mu L_\nu L^\mu L^\nu) + {\rm Tr}(R_\mu R_\nu R^\mu R^\nu)] \\ &\quad + g_4[{\rm Tr}(L_\mu L^\mu L_\nu L^\nu) + {\rm Tr}(R_\mu R^\mu R_\nu R^\nu)] \\ &\quad + g_5\,{\rm Tr}(L_\mu L^\mu)\ {\rm Tr}(R_\nu R^\nu) \\ &\quad + g_6[{\rm Tr}(L_\mu L^\mu)\ {\rm Tr}(L_\nu L^\nu) + {\rm Tr}(R_\mu R^\mu)\ {\rm Tr}(R_\nu R^\nu)], \quad (3)\end{aligned}$$

$$\begin{aligned}\mathcal{L}_{\rm Int} &= \frac{h_1}{2}{\rm Tr}(\Phi^\dagger\Phi)\,{\rm Tr}\left(L_\mu^2+R_\mu^2\right) \\ &\quad + h_2\,{\rm Tr}[|L_\mu\Phi|^2 + |\Phi R_\mu|^2] + 2h_3\,{\rm Tr}(L_\mu\Phi R^\mu\Phi^\dagger), \quad (4)\\ \mathcal{L}_{U(1)_A} &= c[{\rm Det}(\Phi) + {\rm Det}(\Phi^\dagger)] + c_0[{\rm Det}(\Phi) - {\rm Det}(\Phi^\dagger)]^2 \\ &\quad + c_1[{\rm Det}(\Phi) + {\rm Det}(\Phi^\dagger)]\,{\rm Tr}[\Phi\Phi^\dagger]. \quad (5)\end{aligned}$$

The first Lagrangian, Eq. (2), represents kinetic and potential terms for the scalar meson nonets. The third term stands for the explicit symmetry breaking defined in Eq. (10). This Lagrangian creates scalar and pseudoscalar mesonic states defined in Φ nonets; see Eq. (9). The second Lagrangian, Eq. (3), represents the vector meson nonets involving explicit symmetry breaking in the second term defined in Eq. (10). The 3×3 matrix of the vector meson nonets involves vector and axial-vector fields; see Eq. (9). This creates the vector and axial-vector mesonic states and the interactions between the (pseudo)scalar and (axial) vector introduced in Eq. (4). As the symmetry is broken, explicitly and spontaneously, the anomaly term $\mathcal{L}_{U(1)_A}$ in $SU(3)_r\times SU(3)_\ell$ should be introduced into the effective Lagrangian, and c, c_0, c_1 are the parameters to be determined experimentally [38]. The first two terms approximate the original axial anomaly term [53,54], while the

third term is a mixed one. It is proportional to the first term. The concept of choosing the first anomaly term is essential; other terms are used to compare with other effects of the different anomaly terms on the hadronic structure [52].

To describe experimental data, large-order terms with local chiral symmetry should be included [38]. It is worthwhile to highlight that $\mathcal{L}_{\mathrm{U}(1)_A}$ symmetry in the QCD Lagrangian is anomalous [55], known as the QCD vacuum anomaly [23,55], i.e., broken by quantum effects. Without anomaly a ninth pseudoscalar Goldstone boson corresponding to the spontaneous breaking of the chiral $\mathrm{U}(3)_\ell \times \mathrm{U}(3)_r$ symmetry should unfold [23,55]. It is apparent that the hadron theory is not fundamental. Thus, it is assumed to be valid at mass scale of 1–2 GeV [38] and therefore the local chiral symmetry would not cause big problems. Nevertheless, the constraint terms are conjectured to affect such QCD approaches [38]. This well-known $\mathcal{L}_{\mathrm{U}(1)_A}$ problem of QCD is effectively controlled by the anomaly term c in the Lagrangian [56]. The squared tree-level masses of mesons m^2 and m_1^2 contain a contribution arising from the spontaneous symmetry breaking [38].

The introduction of scalar and vector meson nonets into the Lagrangian of PLSM requires redefinition for the contracovariant derivative of the quark meson contribution represented in Eq. (6), where the degrees of freedom of scalar Φ and vector L^μ and R^μ meson nonets are coupling to the electromagnetic field A^μ. Equations (7) and (8) are the left-handed and right-handed field strength tensors, respectively. They represent the self-interaction between the vector and axial-vector mesons with the electromagnetic field A^μ. The local chiral invariance emerging from the globally invariant PLSM Lagrangian requires that $g_1 = g_2 = g_3 = g_4 = g_5 = g_6 = g$ [38]:

$$D^\mu \Phi \equiv \partial^\mu \Phi - i g_1 (L^\mu \Phi - \Phi R^\mu) - i e A^\mu [T_3, \Phi], \tag{6}$$

$$L^{\mu\nu} \equiv \partial^\mu L^\nu - i e A^\mu [T_3, L^\nu] - \{\partial^\nu L^\mu - i e A^\nu [T_3, L^\mu]\}, \tag{7}$$

$$R^{\mu\nu} \equiv \partial^\mu R^\nu - i e A^\mu [T_3, R^\nu] - \{\partial^\nu R^\mu - i e A^\nu [T_3, R^\mu]\}. \tag{8}$$

It is apparent that $T_a = \hat{\lambda}_a/2$ with $a = 0, \ldots, 8$ are nine U(3) generators, where $\hat{\lambda}_a$ are the Gell-Mann matrices with the fields Φ of a 3×3 complex matrix comprising the scalars σ_a ($J^{PC} = 0^{++}$), pseudoscalars π_a ($J^{PC} = 0^{-+}$), V_a^μ vector ($J^{PC} = 1^{-01}$), and A_a^μ axial-vector ($J^{PC} = 1^{++}$) meson states given by

$$\Phi = \sum_{a=0}^{8} T_a (\sigma_a + i\pi_a),$$

$$L^\mu = \sum_{a=0}^{8} T_a \left(V_a^\mu + A_a^\mu\right), \tag{9}$$

$$R^\mu = \sum_{a=0}^{8} T_a \left(V_a^\mu - A_a^\mu\right).$$

$\lambda_0 = \sqrt{\frac{2}{3}}\,\mathbf{1}$ and T_a are normalized such that they obey the U(3) algebra [57]. The chiral symmetry is explicitly broken by

$$H = \sum_{a=0}^{8} T_a h_a, \quad \Delta = \sum_{a=0}^{8} T_a \delta_a. \tag{10}$$

The symmetry breaking terms originate by $\mathrm{U}(3)_L \times \mathrm{U}(3)_R = \mathrm{U}(3)_V \times \mathrm{U}(3)_A$. The terms are proportional to the matrix H and Δ as given in Eq. (10). This relation describes the explicit symmetry breaking due to

(i) finite quark masses in the (pseudo)scalar and (axial)-vector sectors,
(ii) breaking $\mathrm{U}(3)_A$ if $H_0, \Delta_0 \neq 0$, and
(iii) breaking $\mathrm{U}(3)_V \to \mathrm{SU}(2)_V \times \mathrm{U}(1)_V$ if $H_8, \Delta_8 \neq 0$.

For more details, the readers are referred to Ref. [45]. It is conjectured that the spontaneous chiral symmetry breaking takes part in the vacuum state. Therefore, finite vacuum expectation values for the fields Φ and $\bar{\Phi}$ are assumed to carry the quantum numbers of the vacuum [49]. As a result, the components of the explicit symmetry breaking term (diagonal) are h_0, h_3, and h_8, and δ_0, δ_3, and δ_8 should not vanish [49]. This leads to extracting three finite condensates $\bar{\sigma_0}$, $\bar{\sigma_3}$, and $\bar{\sigma_8}$. On the other hand, $\bar{\sigma_3}$ breaks the isospin symmetry SU(2) [49]. To avoid this situation, we restrict ourselves to SU(3). This can be the $N_f = 2 + 1$ [23] flavor pattern. Correspondingly, two degenerate light (up quark and down quark) and one heavier quark flavors (strange quark), i.e., $m_u = m_d \neq m_s$ are assumed. Furthermore, the violation of the isospin symmetry is neglected. This facilitates the choice of h_a ($h_0 \neq 0$, $h_3 = 0$, and $h_8 \neq 0$) and for δ_a ($\delta_0 \neq 0$, $\delta_3 = 0$, and $\delta_8 \neq 0$):

$$T_a\,\sigma_a = \frac{1}{\sqrt{2}} \begin{pmatrix} \frac{1}{\sqrt{2}}\,a_0^0 + \frac{1}{\sqrt{6}}\,\sigma_8 + \frac{1}{\sqrt{3}}\,\sigma_0 & a_0^- & \kappa^- \\ a_0^+ & -\frac{1}{\sqrt{2}}\,a_0^0 + \frac{1}{\sqrt{6}}\,\sigma_8 + \frac{1}{\sqrt{3}}\,\sigma_0 & \bar{\kappa}^0 \\ \kappa^+ & \kappa^0 & -\sqrt{\frac{2}{3}}\,\sigma_8 + \frac{1}{\sqrt{3}}\,\sigma_0 \end{pmatrix}, \tag{11}$$

$$T_a\,\pi_a = \frac{1}{\sqrt{2}} \begin{pmatrix} \frac{1}{\sqrt{2}}\,\pi^0 + \frac{1}{\sqrt{6}}\,\pi_8 + \frac{1}{\sqrt{3}}\,\pi_0 & \pi^- & K^- \\ \pi^+ & -\frac{1}{\sqrt{2}}\,\pi^0 + \frac{1}{\sqrt{6}}\,\pi_8 + \frac{1}{\sqrt{3}}\,\pi_0 & \bar{K}^0 \\ K^+ & K^0 & -\sqrt{\frac{2}{3}}\,\pi_8 + \frac{1}{\sqrt{3}}\,\pi_0 \end{pmatrix}, \tag{12}$$

and

$$T_a\, V_a^\mu = \frac{1}{\sqrt{2}} \begin{pmatrix} \frac{\omega_0+\rho^0}{\sqrt{2}} & \rho^+ & K^{\star+} \\ \rho^- & \frac{\omega_0-\rho^0}{\sqrt{2}} & K^{\star 0} \\ K^{\star-} & \bar{K}^{\star 0} & \omega_8 \end{pmatrix}^\mu , \tag{13}$$

$$T_a\, A_a^\mu = \frac{1}{\sqrt{2}} \begin{pmatrix} \frac{f_{1_0}+a_1^0}{\sqrt{2}} & a_1^+ & K_1^+ \\ a_1^- & \frac{f_{1_0}-a_1^0}{\sqrt{2}} & K_1^0 \\ K_1^- & \bar{K}_1^0 & f_{1_8} \end{pmatrix}^\mu . \tag{14}$$

It would be more convenient to convert the condensates σ_0 and σ_8 into a pure non-strange σ_x and a pure strange σ_y quark flavor [58]:

$$\begin{pmatrix} \sigma_x \\ \sigma_y \end{pmatrix} = \frac{1}{\sqrt{3}} \begin{pmatrix} \sqrt{2} & 1 \\ 1 & -\sqrt{2} \end{pmatrix} \begin{pmatrix} \sigma_0 \\ \sigma_8 \end{pmatrix}. \tag{15}$$

It is worthwhile to mention that $\sigma \ni (\sigma_a, \pi_a, V_a^\mu, A_a^\mu)$.

A. Polyakov-loop potential

The Lagrangian of LSM can be coupled to the Polyakov-loop dynamics [16,23]:

$$\mathcal{L} = \mathcal{L}_{\rm chiral} - \mathcal{U}(\phi, \phi^*, T). \tag{16}$$

The second term in Eq. (16), $\mathcal{U}(\phi, \phi^*, T)$, represents the effective Polyakov-loop potential [5], which gives the dynamics of the thermal expectation value of a color-traced Wilson loop in the temporal direction [5]:

$$\phi(\vec{x}) = \frac{1}{N_c} \langle \mathcal{P}(\vec{x}) \rangle. \tag{17}$$

Then, the Polyakov-loop potential and its conjugate read

$$\phi = \langle {\rm Tr}_c\, \mathcal{P} \rangle / N_c, \quad \phi^* = \langle {\rm Tr}_c\, \mathcal{P}^\dagger \rangle / N_c, \tag{18}$$

where $\mathcal{P}$ is the Polyakov loop, which can be expressed as a matrix in the color space [5],

$$\mathcal{P}(\vec{x}) = \mathcal{P} \exp\left[i \int_0^\beta d\tau\, A_0(\vec{x}, \tau) \right], \tag{19}$$

where $\beta = 1/T$ is the inverse temperature and A_0 is the temporal component of Euclidean vector field [5,6]. The Polyakov-loop matrix can be reexpressed as a diagonal representation [59], as in Eq. (18), where the gauge filed $A_\mu = g_s\, A_\mu^a\, \lambda^a/2$ with $a = 1, \ldots, N_c^2 - 1$ and g_s being the gauge coupling.

The coupling between the Polyakov loop and the quarks is unrivaled and is given by the covariant derivative $D_\mu = \partial_\mu - i\, A_\mu$, Eq. (16), where $A_\mu = \delta_{\mu 0}\, A_0$ is given in the chiral limit, Eq. (16), and therefore is invariant under the chiral flavor group. This is the same as the QCD Lagrangian [60–62]. In order to reproduce the thermodynamic behavior of the Polyakov loop for the pure gauge, we use the temperature-dependent potential $U(\phi, \phi^*, T)$, which agrees with lattice QCD calculations and has $Z(3)$ center symmetry [42,60–62] like the pure gauge QCD Lagrangian [42,60]. In case of no quarks, $\phi = \phi^*$ and the Polyakov loop is considered as an order parameter for the deconfinement phase-transition [42,60]. In the present work, we use $U(\phi, \phi^*, T)$ as a polynomial expansion in ϕ and ϕ^* [42,60–62],

$$\frac{\mathcal{U}_{\rm poly}(\phi, \phi^*, T)}{T^4} = -\frac{b_2(T)}{4}(|\phi|^2 + |\phi^*|^2) - \frac{b_3}{6}(\phi^3 + \phi^{*3}) + \frac{b_4}{16}(|\phi|^2 + |\phi^*|^2)^2, \tag{20}$$

where $b_2(T) = a_0 + a_1\,(T_0/T) + a_2\,(T_0/T)^2 + a_3\,(T_0/T)^3$. To reproduce the pure gauge QCD thermodynamics and the behavior of the Polyakov loop as a function of temperature, we use the parameters $a_0 = 6.75$, $a_1 = -1.95$, $a_2 = 2.625$, $a_3 = -7.44$, $b_3 = 0.75$, and $b_4 = 7.5$ [60]. Accordingly, the deconfinement temperature, $T_0 = 270$ MeV, in the pure gauge sector.

B. Mean field approximation

The partition function can be constructed, when taking into consideration a spatially uniform system in a thermal equilibrium at finite temperature T and finite quark chemical potential μ_f, where f stands for u, d and s quarks. The change in particles and antiparticles is governed by the grand canonical partition function. A path integral over the quark, antiquark and meson fields leads to [23]

$$\begin{aligned} \mathcal{Z} &= {\rm Tr} \exp\left[-\left(\hat{\mathcal{H}} - \sum_{f=u,d,s} \mu_f \hat{\mathcal{N}}_f \right) \Big/ T \right] \\ &= \int \prod_a \mathcal{D}\sigma_a \mathcal{D}\pi_a \int \mathcal{D}\psi\, \mathcal{D}\bar{\psi} \\ &\quad \times \exp\left[\int_x \left(\mathcal{L} + \sum_{f=u,d,s} \mu_f \bar{\psi}_f \gamma^0 \psi_f \right) \right], \end{aligned} \tag{21}$$

where $\int_x \equiv i \int_0^{1/T} dt \int_V d^3x$ and V is the volume of the system. For a symmetric quark matter, the uniform blind chemical potential fulfills the conditions that $\mu_f \equiv \mu_u = \mu_d = \mu_s$ [23,63,64]. The meson fields can be replaced by their expectation values $\bar{\sigma_x}$ and $\bar{\sigma_y}$ [65]. In estimating the integration over the fermions yields, other methods were introduced [65]. The effective mesonic potential can be deduced and the thermodynamic potential density reads

$$\Omega(T, \mu) = \frac{-T \ln \mathcal{Z}}{V} = U(\sigma_x, \sigma_y) + \mathcal{U}(\phi, \phi^*, T) + \Omega_{\bar{q}q}(T, \mu_f). \tag{22}$$

The explicit quark contribution to the LSM is given as

$$\Omega_{\bar{q}q}(T, \mu_f) = \nu_c T \sum_{f=u,d,s} \int_0^\infty \frac{d^3k}{(2\pi)^3} \{ \ln[1 - n_{q,f}(T, \mu_f)] + \ln[1 - n_{\bar{q},f}(T, \mu_f)] \}, \tag{23}$$

with the usual fermionic occupation numbers (for quarks) $n_{q,f}(T, \mu_f) = \{1 + \exp[(E_f - \mu_f)/T]\}^{-1}$. For antiquarks $n_{\bar{q},f}(T, \mu_f) \equiv n_{q,f}(T, -\mu_f)$. The number of internal quark degrees of freedom is denoted by $\nu_c = 2N_c = 6$. The flavor-dependent single-particle energies are given as $E_f = (k^2 + m_f^2)^{1/2}$, where m_f is the flavor-dependent quark masses. Also,

the light quark sector is conjectured to decouple from the strange quark sector [42]. Assuming degenerate light quarks, i.e., $l \equiv u,d$, then the masses can be simplified as [58]

$$m_l = g\frac{\sigma_x}{2}, \quad m_s = g\frac{\sigma_y}{\sqrt{2}}. \tag{24}$$

For PLSM, the quarks and antiquarks contributions to the potential are given as [65]

$$\begin{aligned}\Omega_{\bar{q}q}(T,\mu) &= -\nu_c\, T \sum_{f=l,s} \int_0^\infty \frac{d^3\vec{p}}{(2\pi)^3} \{\ln[1+3(\phi+\phi^* e^{-(E_f-\mu)/T}) \\ &\times e^{-(E_f-\mu)/T} + e^{-3(E_f-\mu)/T}] \\ &+ \ln[1+3(\phi^*+\phi e^{-(E_f+\mu)/T}) \\ &\times e^{-(E_f+\mu)/T} + e^{-3(E_f+\mu)/T}]\},\end{aligned} \tag{25}$$

Based on nonstrange σ_x and strange σ_y condensates and taking into consideration Eq. (15), then the purely mesonic potential reads

$$\begin{aligned}U(\sigma_x,\sigma_y) = &-h_x\sigma_x - h_y\sigma_y + \frac{m^2}{2}\left(\sigma_x^2+\sigma_y^2\right) - \frac{c}{2\sqrt{2}}\sigma_x^2\sigma_y \\ &+ \frac{\lambda_1}{2}\sigma_x^2\sigma_y^2 + \frac{1}{8}(2\lambda_1+\lambda_2)\sigma_x^4 + \frac{1}{4}(\lambda_1+\lambda_2)\sigma_y^4.\end{aligned}$$

III. PHASE TRANSITIONS AND THEIR ORDER PARAMETERS

By minimizing the thermodynamic potential, Eq. (22), with respective to σ_x, σ_y, ϕ, and ϕ^*, we obtain a set of four equations of motion σ_x, σ_y, ϕ, and ϕ^*:

$$\frac{\partial\Omega}{\partial\sigma_x} = \frac{\partial\Omega}{\partial\sigma_y} = \frac{\partial\Omega}{\partial\phi} = \frac{\partial\Omega}{\partial\phi^*}\bigg|_{\sigma_x=\bar{\sigma_x},\sigma_y=\bar{\sigma_y},\phi=\bar{\phi},\,\phi^*=\bar{\phi^*}} = 0, \tag{26}$$

with $\sigma_x = \bar{\sigma_x}$, $\sigma_y = \bar{\sigma_y}$, $\phi = \bar{\phi}$, and $\phi^* = \bar{\phi^*}$ being the global minimum, where all thermodynamics quantities are related to the parameters σ_x, σ_y, ϕ, and ϕ^*.

In order to determine the chiral phase transition, σ_x and σ_y, and the deconfinement phase transition, ϕ and ϕ^* should be estimated. The chiral mesonic phase structures in temperature and density dependence are taken as free parameters to be fitted experimentally. These parameters are classified corresponding to scalar meson nonets m^2, h_x, h_y, λ_1, λ_2, and c [23]. The vector meson nonets have the parameters m_1^2, g_1, h_1, h_2, h_3, δ_x, and δ_y [36].

In the present work we use $\sigma = 800$ MeV. At vanishing temperature, the chiral condensates for light and strange quarks are taken as $\sigma_{x_0} = 92.4$ MeV and $\sigma_{y_0} = 94.5$ MeV, respectively [16,23]. These values are used to normalize their thermal evolution at vanishing chemical potential. In this limit, the two Polyakov loops are identical, i.e., $\langle\phi\rangle = \langle\phi^*\rangle$. To determining the critical temperature of the phase transition (crossover), two approaches can be implemented:

(i) The first one is the point at which the order parameter intersects with the curve of the corresponding chiral condensate.
(ii) The second one is based on the maxima/peaks of the temperature derivative of the condensates (chiral susceptibilities) for strange and nonstrange quarks. The peaks should be ordered to the critical temperatures.

The first approach was used to derive the results depicted in Fig. 1. Accordingly, we find that the chiral restoration of the nonstrange condensate is related to $T_c^q \sim 181$ MeV, while for the strange quark to $T_c^s \sim 270$ MeV.

The lattice QCD simulations prefer dimensionless quantities. Therefore, the chiral order parameter is expressed in the chiral condensate [66]:

$$M_b = \frac{m_s\langle\bar{\sigma_x}(T,\mu)\rangle}{T^4}. \tag{27}$$

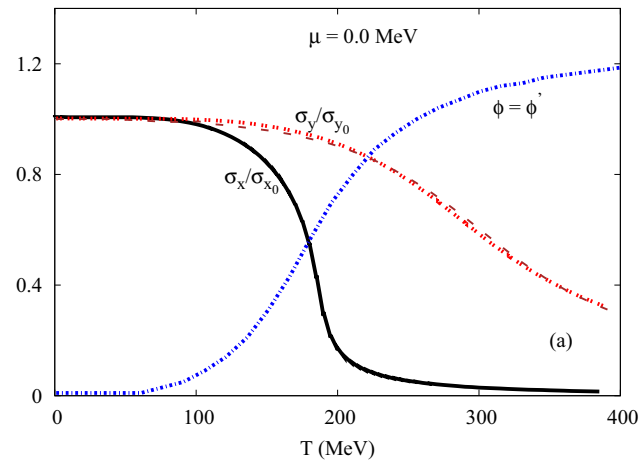

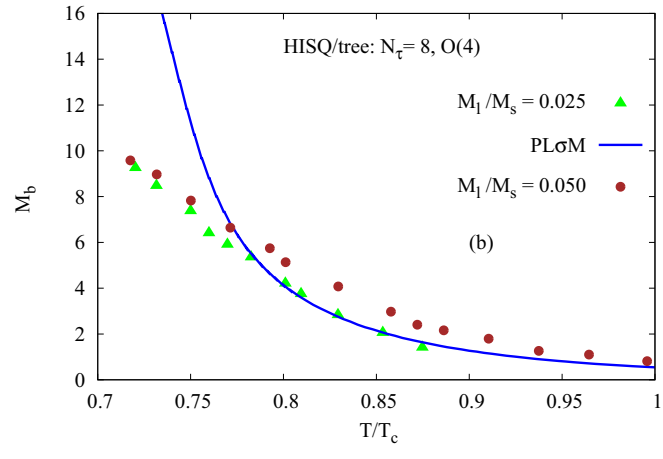

FIG. 1. (Color online) Left-hand panel: the chiral condensates σ_x and σ_y (solid and dotted curves, respectively) and the Polyakov loops ϕ and ϕ^* (dashed curve at $c = 0$, i.e., without anomaly) are given as functions of the temperature at vanishing baryon chemical potential. At $\mu = 0$ MeV, the two Polyakov loops are identical, i.e., $\phi = \phi^*$. Right-hand panel: the chiral condensate in $\mathcal{O}(4)$ lattices [66] with HISQ/tree with $N_t = 8$ is compared with the PLSM calculations (solid curve). The rectangular symbols stand for $M_q/M_s = 0.025$ and the circular ones represent $M_q/M_s = 0.05$.

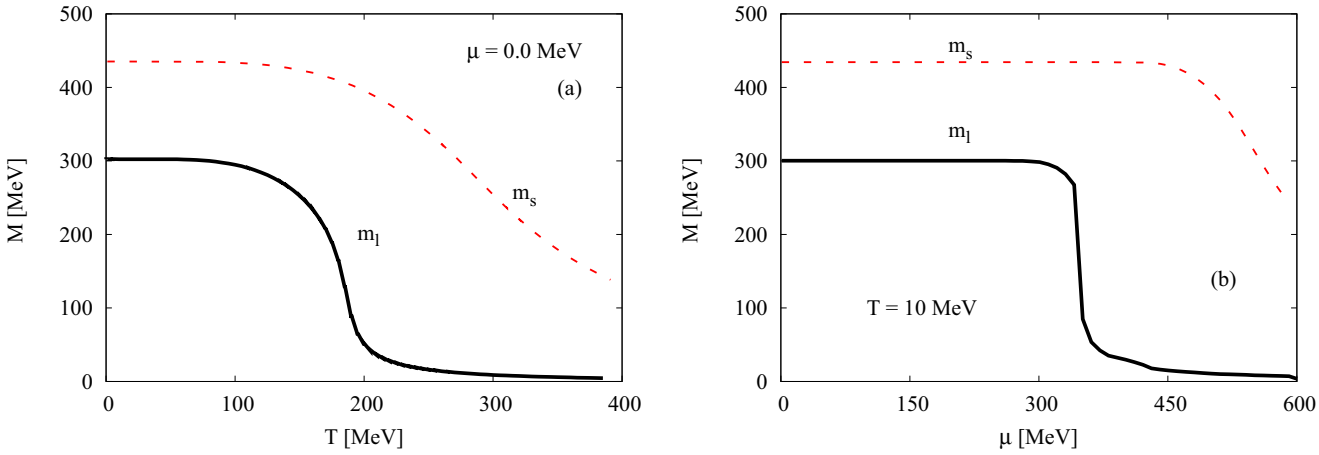

FIG. 2. (Color online) The left-hand panel presents the thermal evolution of nonstrange m_l (solid curve) and strange m_s (dashed curve) at $\mu = 0$ MeV. The right-hand panel shows their dependence on the baryon chemical potential at a fixed temperature $T = 10$ MeV.

The right-hand panel of Fig. 1 compares the chiral condensate from the highly improved staggered quark action plus tree-level action (HISQ/tree) with temporal dimensions $N_t = 8$, and two quark masses $M_q/M_s = 0.025$ and $M_q/M_s = 0.05$ in $\mathcal{O}(4)$ lattices [66] with the PLSM calculations for M_b; see Eq. (27).

When the light constituent quark mass takes the value $m_l = 300$ MeV, the coupling $g = 6.5$ and the strange constituent quark mass reads $m_s \sim 433$ MeV. These are normalized to the values at zero temperature T and vanishing baryon chemical potential μ. In cases of finite T and vanishing μ, and vanishing T and finite μ, the chiral phase transition is determined by nonstrange and strange quarks fields, Eq. (24), as shown in Fig. 2. The left-hand panel of Fig. 2 shows the thermal evolution of nonstrange and strange quarks at vanishing μ. The right-hand panel shows their density dependence at $T = 10$ MeV. The contribution of finite quark mass seems to have a considerable effect on the chiral phase transition. To this end, the normalized condensates are studied in T and μ dependence.

For the in-medium thermal and density effects on the mesonic masses, we present in the left-hand panel of Fig. 3 the chiral condensates at varying temperatures and fixed baryon chemical potentials. In doing this, we take into consideration the thermal and density dependences of the chiral condensates. For instance, we present the chiral condensates at different temperatures and chemical potentials. At these temperatures and chemical potentials, we should estimate the thermal and density dependences of the mesonic states. We notice that the values of σ_x and σ_y decrease with increasing T. There is a rapid decrease within a narrow range of temperatures. The light quarks are more sensitive than the strange quarks. This likely describes the characteristics of the chiral phase transition.

There is a similar decrease in both quantities with increasing hadronic dense medium (baryon chemical potential), seen in the right-hand panel of Fig. 3. We notice that the sudden decrease around the chiral phase transition is sharper than the one in the left-hand panel. This would indicate that the chiral phase transition at large density and low temperature

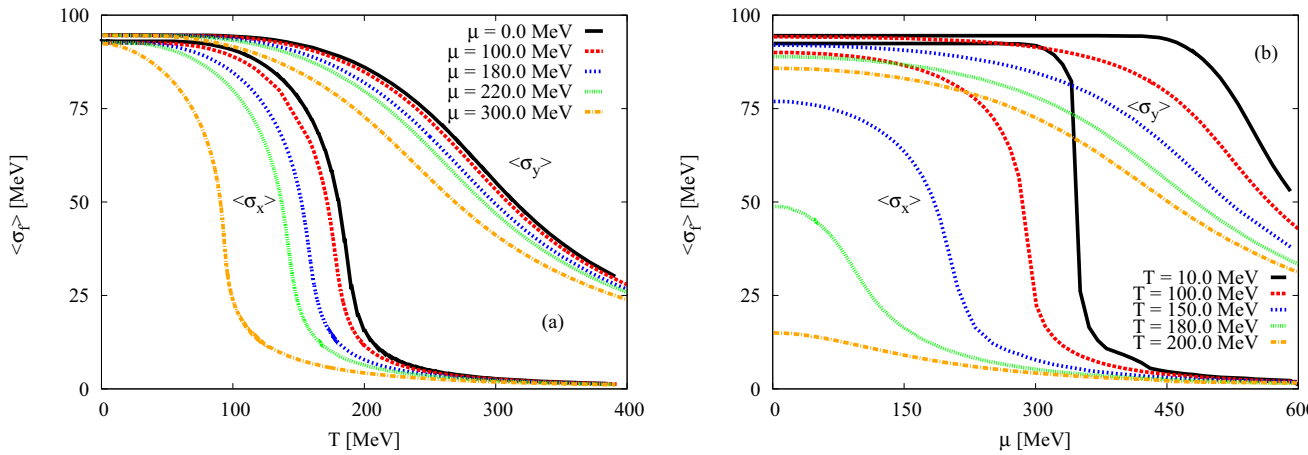

FIG. 3. (Color online) Left-hand panel: the averaged chiral condensate, $\langle\sigma_x\rangle$, is given as functions of temperature at different chemical potentials $\mu = 0$, 100, 180, 200, and 300 MeV (solid curves from top to bottom, respectively). For the chiral condensate $\langle\sigma_y\rangle$ we fix the same values of μ. The right-hand panel presents the dependence on μ, where the temperatures are fixed at the given values $T = 10$, 100, 150, 180, and 200 MeV (solid curves from top to bottom, respectively).

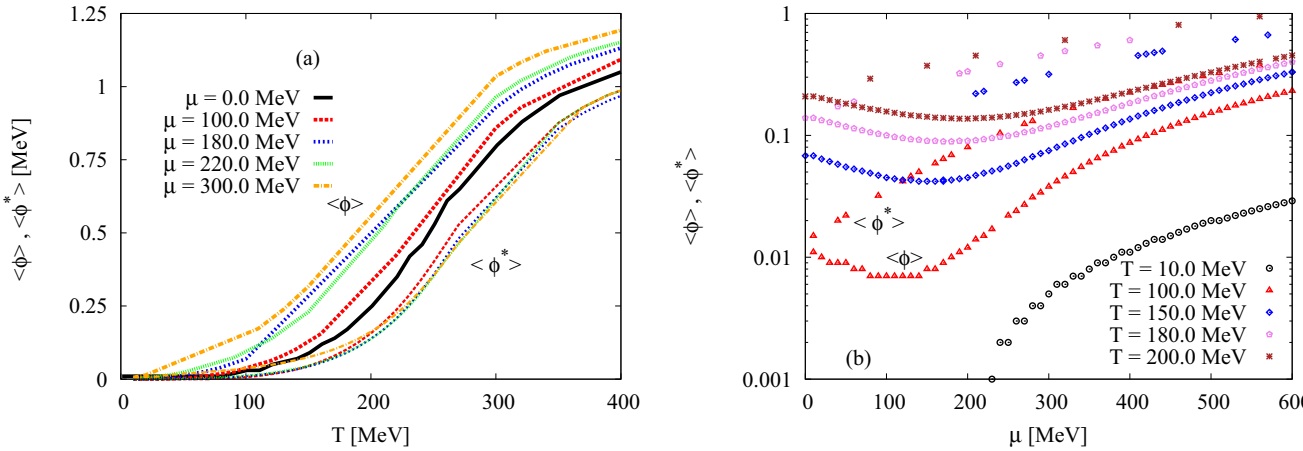

FIG. 4. (Color online) The expectation values of the Polyakov-loop fields, ϕ and ϕ^* (left-hand panel), are given as functions of temperature at different chemical potentials $\mu = 0$, 100, 180, 200, and 300 MeV for ϕ^* (upward from the solid curve) and for ϕ (downward from the solid curve). The chiral condensates, ϕ and ϕ^* (right-hand panel), are given as functions of the chemical potential numerically in logarithmic scale at different temperatures $T = 10$, 100, 150, 180, and 200 MeV as points: ϕ (top curves) and ϕ^* (bottom curves).

(very near to the abscissa of the QCD phase diagram [67]) is more prompt than the one at low chemical potential and high temperature. The earlier would likely be characterized as a first-order phase transition, while the latter as a moderate phase transition (crossover) [67,68].

We also notice that the fast decrease of σ_x takes place earlier and faster than that of σ_y. For instance, in the left-hand panel of Fig. 2, we find that $T_c^q = 181$ MeV at vanishing density, and the decreases are smooth, while at finite baryon chemical density and fixed $T = 10$ MeV the critical value $\mu = 360$ MeV. This would be interpreted as a *smooth* phase transition know as crossover [69]. Thus, in presence of the Polyakov-loop potential, UA(1) of the symmetry breaking term is kept constant throughout the chiral and deconfinement phase transition.

For the results depicted in Fig. 4, we analyze the deconfinement phase transition at varying baryon chemical potentials and temperatures and include the Polyakov-loop corrections to the meson masses at five different fixed temperatures and five different chemical potentials. The thermal effects of the hadronic medium on the evolution of ϕ seem to be very smooth. In hadronic dense medium, the slope of $\phi(\mu)$ seems to depend on the temperature. It is always positive and increases rapidly with μ, while $\phi(\mu)^*$ decreases slowly compared to $\phi(\mu)$. Both quantities intersect at a characteristic value of μ depending on value of the temperature T.

IV. MASSES OF SIXTEEN MESONIC STATES

A. Inclusion of anomalous terms

It is assumed that the contribution of the quark potential to the Lagrangian vanishes in the vacuum. Therefore, the meson potential determines the mass matrix, entirely. In other words, the meson masses do not receive any contribution from quarks or antiquarks in vacuum. Thus, the meson masses are governed by the meson potential [23,45].

The masses are defined by the second derivative of the grand potential $\Omega(T,\mu_f)$, Eq. (22), evaluated at its minimum Eq. (28), with respect to the corresponding fields. In the present calculations, the minima are estimated by vanishing expectation values of all scalar, pseudoscalar, vector, and axial-vector fields. The pure strange $\bar{\sigma}_x$ and nonstrange $\bar{\sigma}_y$ condensates are finite,

$$m^2_{i,ab} = \left.\frac{\partial^2\Omega(T,\mu_f)}{\partial\zeta_{i,a}\partial\zeta_{i,b}}\right|_{\min}, \tag{28}$$

where i stands for scalar, pseudoscalar, vector, and axial-vector mesons and a and b range $0,\ldots,8$. In vacuum, the mesonic sectors are formulated in the nonstrange and strange basis:

(i) Scalar meson masses are given as

$$m^2_{a_0} = m^2 + \lambda_1\left(\bar{\sigma}_x^2 + \bar{\sigma}_y^2\right) + \frac{3\lambda_2}{2}\bar{\sigma}_x^2 + \frac{\sqrt{2}c}{2}\bar{\sigma}_y, \tag{29}$$

$$m^2_{\kappa} = m^2 + \lambda_1\left(\bar{\sigma}_x^2 + \bar{\sigma}_y^2\right) + \frac{\lambda_2}{2}\left(\bar{\sigma}_x^2 + \sqrt{2}\bar{\sigma}_x\bar{\sigma}_y + 2\bar{\sigma}_y^2\right) + \frac{c}{2}\bar{\sigma}_x, \tag{30}$$

$$m^2_{\sigma} = m^2_{s,00}\cos^2\theta_s + m^2_{s,88}\sin^2\theta_s + 2m^2_{s,08}\sin\theta_s\cos\theta_s, \tag{31}$$

$$m^2_{f_0} = m^2_{s,00}\sin^2\theta_s + m^2_{s,88}\cos^2\theta_s - 2m^2_{s,08}\sin\theta_s\cos\theta_s, \tag{32}$$

with

$$m^2_{s,00} = m^2 + \frac{\lambda_1}{3}\left(7\bar{\sigma}_x^2 + 4\sqrt{2}\bar{\sigma}_x\bar{\sigma}_y + 5\bar{\sigma}_y^2\right) + \lambda_2\left(\bar{\sigma}_x^2 + \bar{\sigma}_y^2\right) - \frac{\sqrt{2}c}{3}(\sqrt{2}\bar{\sigma}_x + \bar{\sigma}_y),$$

$$m^2_{s,88} = m^2 + \frac{\lambda_1}{3}\left(5\bar{\sigma}_x^2 - 4\sqrt{2}\bar{\sigma}_x\bar{\sigma}_y + 7\bar{\sigma}_y^2\right) + \lambda_2\left(\frac{\bar{\sigma}_x^2}{2} + 2\bar{\sigma}_y^2\right) + \frac{\sqrt{2}c}{3}\left(\sqrt{2}\bar{\sigma}_x - \frac{\bar{\sigma}_y}{2}\right),$$

$$m_{s,08}^2 = \frac{2\lambda_1}{3}\left(\sqrt{2}\bar{\sigma}_x^2 - \bar{\sigma}_x\bar{\sigma}_y - \sqrt{2}\bar{\sigma}_y^2\right) + \sqrt{2}\lambda_2\left(\frac{\bar{\sigma}_x^2}{2} - \bar{\sigma}_y^2\right) + \frac{c}{3\sqrt{2}}(\bar{\sigma}_x - \sqrt{2}\bar{\sigma}_y),$$

and s (scalar) refers to i in Eq. (28).

(ii) Pseudoscalar meson masses read

$$m_\pi^2 = m^2 + \lambda_1\left(\bar{\sigma}_x^2 + \bar{\sigma}_y^2\right) + \frac{\lambda_2}{2}\bar{\sigma}_x^2 - \frac{\sqrt{2}c}{2}\bar{\sigma}_y, \quad (33)$$

$$m_K^2 = m^2 + \lambda_1\left(\bar{\sigma}_x^2 + \bar{\sigma}_y^2\right) + \frac{\lambda_2}{2}\left(\bar{\sigma}_x^2 - \sqrt{2}\bar{\sigma}_x\bar{\sigma}_y + 2\bar{\sigma}_y^2\right) - \frac{c}{2}\bar{\sigma}_x, \quad (34)$$

$$m_{\eta'}^2 = m_{p,00}^2\cos^2\theta_p + m_{p,88}^2\sin^2\theta_p + 2m_{p,08}^2\sin\theta_p\cos\theta_p, \quad (35)$$

$$m_\eta^2 = m_{p,00}^2\sin^2\theta_p + m_{p,88}^2\cos^2\theta_p - 2m_{p,08}^2\sin\theta_p\cos\theta_p, \quad (36)$$

with

$$m_{p,00}^2 = m^2 + \lambda_1\left(\bar{\sigma}_x^2 + \bar{\sigma}_y^2\right) + \frac{\lambda_2}{3}\left(\bar{\sigma}_x^2 + \bar{\sigma}_y^2\right) + \frac{c}{3}(2\bar{\sigma}_x + \sqrt{2}\bar{\sigma}_y),$$

$$m_{p,88}^2 = m^2 + \lambda_1\left(\bar{\sigma}_x^2 + \bar{\sigma}_y^2\right) + \frac{\lambda_2}{6}\left(\bar{\sigma}_x^2 + 4\bar{\sigma}_y^2\right) - \frac{c}{6}(4\bar{\sigma}_x - \sqrt{2}\bar{\sigma}_y),$$

$$m_{p,08}^2 = \frac{\sqrt{2}\lambda_2}{6}\left(\bar{\sigma}_x^2 - 2\bar{\sigma}_y^2\right) - \frac{c}{6}(\sqrt{2}\bar{\sigma}_x - 2\bar{\sigma}_y);$$

the mixing angles are given by

$$\tan 2\theta_i = \frac{2m_{i,08}^2}{m_{i,00}^2 - m_{i,88}^2}, \quad i = s,p, \quad (37)$$

and p (pseudoscalar) refers to i in Eq. (28).

(iii) Vector meson masses are given as

$$m_\rho^2 = m_1^2 + \frac{1}{2}(h_1 + h_2 + h_3)\bar{\sigma}_x^2 + \frac{h_1}{2}\bar{\sigma}_y^2 + 2\delta_x, \quad (38)$$

$$m_{K^\star}^2 = m_1^2 + \frac{\bar{\sigma}_x^2}{4}\left(g_1^2 + 2h_1 + h_2\right) + \frac{\bar{\sigma}_x\bar{\sigma}_y}{\sqrt{2}}\left(h_3 - g_1^2\right) + \frac{\bar{\sigma}_y^2}{2}\left(g_1^2 + h_1 + h_2\right) + \delta_x + \delta_y, \quad (39)$$

$$m_{\omega_x}^2 = m_\rho^2, \quad (40)$$

$$m_{\omega_y}^2 = m_1^2 + \frac{h_1}{2}\bar{\sigma}_x^2 + \left(\frac{h_1}{2} + h_2 + h_3\right)\bar{\sigma}_y^2 + 2\delta_y, \quad (41)$$

and vectors V^μ refer to i in Eq. (28).

(iv) And finally the axial-vectors masses are

$$m_{a_1}^2 = m_1^2 + \frac{1}{2}\left(2g_1^2 + h_1 + h_2 - h_3\right)\bar{\sigma}_x^2 + \frac{h_1}{2}\bar{\sigma}_y^2 + 2\delta_x, \quad (42)$$

$$m_{K_1}^2 = m_1^2 + \frac{1}{4}\left(g_1^2 + 2h_1 + h_2\right)\bar{\sigma}_x^2 - \frac{1}{\sqrt{2}}\bar{\sigma}_x\bar{\sigma}_y\left(h_3 - g_1^2\right) + \frac{1}{2}\left(g_1^2 + h_1 + h_2\right)\bar{\sigma}_y^2 + \delta_x + \delta_y, \quad (43)$$

$$m_{f_{1x}}^2 = m_{a_1}^2, \quad (44)$$

$$m_{f_{1y}}^2 = m_1^2 + \frac{\bar{\sigma}_x^2}{2}h_1 + \left(2g_1^2 + \frac{h_1}{2} + h_2 - h_3\right)\bar{\sigma}_y^2 + 2\delta_y, \quad (45)$$

and axialvector A^μ refer to i in Eq. (28).

The evolution of masses of (pseudo)scalar states depends on the anomaly term of $\mathcal{L}_{\mathrm{U}(1)_A}$. This term causes the anomaly in the c term. The way of choosing the anomaly term defines and describes of the structure of the hadronic states [52]. The anomaly term, which we have implemented here, agrees with the calculation of Refs. [23,24,70] but differs from Ref. [38]. Moreover, the estimated masses of (axial-)vector states are not affected by the anomaly term [38].

The quantum and thermal fluctuations of the mesonic fields are neglected. It is worthwhile to mention that the integration over the mesonic fields is not used. Furthermore, the mesonic fields are replaced by their expectation values, σ_0 and σ_8, resulting in the mesonic potential $U(\sigma_0,\sigma_8)$. The quarks are treated as quantum fields. The integration over the quark fields yields a determinant, which can be rewritten as a trace over a logarithm defined by Eq. (23) for LSM and Eq. (25) for PLSM. The Matsubara formalism [71] gives an estimation for the quark contribution to the meson masses; see Sec. V.

In order to include the quark contribution to the grand potential, the meson masses should be modified due to the in-medium effects. In calculating the second derivative, Eq. (28), we take into account Eq. (23) and diagonalize the resulting quark mass matrix. Then, we can deduce an expression for the modification in the meson masses [23]:

$$m_{i,ab}^2 = \left.\frac{\partial^2\Omega(T,\mu_f)}{\partial\zeta_{i,a}\partial\zeta_{i,b}}\right|_{\min} = \nu_c\sum_{f=l,s}\int\frac{d^3p}{(2\pi)^3}\frac{1}{2E_{q,f}}\left[\left(n_{q,f} + n_{\bar{q},f}\right)\left(m_{f,ab}^2 - \frac{m_{f,a}^2 m_{f,b}^2}{2E_{q,f}^2}\right) - \left(b_{q,f} + b_{\bar{q},f}\right)\left(\frac{m_{f,a}^2 m_{f,b}^2}{2E_{q,f}T}\right)\right]. \quad (46)$$

The quark mass derivative with respect to the meson fields $\zeta_{i,a}, m_{f,a}^2 \equiv \partial m_f^2/\partial\zeta_{i,a}$ and that with respect to the meson fields $\zeta_{i,a}\partial\zeta_{i,b}, m_{f,ab}^2 \equiv \partial m_f^2/\partial\zeta_{i,a}\partial\zeta_{i,b}$ are listed in Table I. Correspondingly, the antiquark function $b_{\bar{q},f}(T,\mu_f) = b_{q,f}(T,-\mu_f)$,

where

$$b_{q,f}(T,\mu_f) = n_{q,f}(T,\mu_f)[1 - n_{q,f}(T,\mu_f)]. \tag{47}$$

An expression for the meson mass modification can be estimated from PLSM, Eq. (25), and the diagonalization of the resulting quark mass matrix [24],

$$m^2_{i,ab} = \left.\frac{\partial^2\Omega(T,\mu_f)}{\partial\zeta_{i,a}\partial\zeta_{i,b}}\right|_{\min} = \nu_c \sum_{f=l,s}\int \frac{d^3p}{(2\pi)^3}\frac{1}{2E_{q,f}}\left[(N_{q,f}+N_{\bar{q},f})\left(m^2_{f,ab} - \frac{m^2_{f,a}m^2_{f,b}}{2E^2_{q,f}}\right) + (B_{q,f}+B_{\bar{q},f})\left(\frac{m^2_{f,a}m^2_{f,b}}{2E_{q,f}T}\right)\right]. \tag{48}$$

In estimating $m^2_{i,ab}$, the definitions $E_{q,f}(T,\mu) = E_{q,f}(T,-\mu)$ and

$$N_{q,f} = \frac{\Phi e^{-E_{q,f}/T} + 2\Phi^* e^{-2E_{q,f}/T} + e^{-3E_{q,f}/T}}{1 + 3(\phi + \phi^* e^{-E_{q,f}/T})e^{-E_{q,f}/T} + e^{-3E_{\bar{q},f}/T}}, \tag{49}$$

$$N_{\bar{q},f} = \frac{\Phi^* e^{-E_{\bar{q},f}/T} + 2\Phi e^{-2E_{\bar{q},f}/T} + e^{-3E_{\bar{q},f}/T}}{1 + 3(\phi^* + \phi e^{-E_{\bar{q},f}/T})e^{-E_{\bar{q},f}/T} + e^{-3E_{\bar{q},f}/T}} \tag{50}$$

are implemented [24]. Furthermore, for quarks $B_{q,f} = 3(N_{q,f})^2 - C_{q,f}$ and for antiquarks $B_{\bar{q},f} = 3(N_{\bar{q},f})^2 - C_{\bar{q},f}$, where

$$C_{q,f} = \frac{\Phi e^{-E_{q,f}/T} + 4\Phi^* e^{-2E_{q,f}/T} + 3e^{-3E_{q,f}/T}}{1 + 3(\phi + \phi^* e^{-E_{q,f}/T})\, e^{-E_{q,f}/T} + e^{-3E_{\bar{q},f}/T}}, \tag{51}$$

$$C_{\bar{q},f} = \frac{\Phi^* e^{-E_{\bar{q},f}/T} + 4\Phi e^{-2E_{\bar{q},f}/T} + 3e^{-3E_{\bar{q},f}/T}}{1 + 3(\phi^* + \phi e^{-E_{\bar{q},f}/T})\, e^{-E_{\bar{q},f}/T} + e^{-3E_{\bar{q},f}/T}} \tag{52}$$

are defined [24].

The quark masses have to be taken into account and accordingly same isospin of light quarks $m_u = m_d$, but different for m_s. The first and second derivatives of squared quark mass in nonstrange and strange basis with respect to meson fields are evaluated at minima [23]. In Table I, the summations over the two light flavors denoted by symbol l are in given in the first two columns, presenting the first and second derivatives of squared light quark masses, respectively.

TABLE I. The first and second derivatives of squared quark masses in nonstrange (first two columns) and strange (last two columns) basis with respect to the meson fields are evaluated at minima [23].

		$m^2_{l,a}m^2_{q,b}/g^4$	$m^2_{l,ab}/g^2$	$m^2_{s,a}m^2_{s,b}/g^4$	$m^2_{s,ab}/g^2$
σ_0	σ_0	$\frac{1}{3}\sigma_x^2$	$\frac{2}{3}$	$\frac{1}{3}\sigma_y^2$	$\frac{1}{3}$
σ_1	σ_1	$\frac{1}{2}\sigma_x^2$	1	0	0
σ_4	σ_4	0	$\sigma_x\frac{\sigma_x+\sqrt{2}\sigma_y}{\sigma_x^2-2\sigma_y^2}$	0	$\sigma_y\frac{\sqrt{2}\sigma_x+2\sigma_y}{2\sigma_y^2-\sigma_x^2}$
σ_8	σ_8	$\frac{1}{6}\sigma_x^2$	$\frac{1}{3}$	$\frac{2}{3}\sigma_y^2$	$\frac{2}{3}$
σ_0	σ_8	$\frac{\sqrt{2}}{6}\sigma_x^2$	$\frac{\sqrt{2}}{3}$	$-\frac{\sqrt{2}}{3}\sigma_y^2$	$-\frac{\sqrt{2}}{3}$
π_0	π_0	0	$\frac{2}{3}$	0	$\frac{1}{3}$
π_1	π_1	0	1	0	0
π_4	π_4	0	$\sigma_x\frac{\sigma_x-\sqrt{2}\sigma_y}{\sigma_x^2-2\sigma_y^2}$	0	$\sigma_y\frac{\sqrt{2}\sigma_x-2\sigma_y}{\sigma_x^2-2\sigma_y^2}$
π_8	π_8	0	$\frac{1}{3}$	0	$\frac{2}{3}$
π_0	π_8	0	$\frac{\sqrt{2}}{3}$	0	$-\frac{\sqrt{2}}{3}$

The last two columns are devoted to the strange quark mass. In spite of the consideration of SU(2) isospin symmetry, the first and second derivatives of squared light quark masses are different for the u and d quarks, where their summation is canceled out [23].

Table II presents a comparison between the different scalar and vector meson nonets in various effective thermal models, such PLSM (present work) and PNJL [27] compared to PDG [33] and lattice QCD calculations [30,31]. Some remarks are now in order. The errors are deduced from the fitting for the parameters used in calculating the equation of states and other thermodynamics quantities. The fitting requires information from the experimental inputs about (axial-)vector and (pseudo)scalar states. The output results are very precise for some light hadrons described by the present model, the PLSM. We aim to describe hadron vacuum phenomenology with such extreme precision and not only to describe the hadron spectrum in both thermal and hadronic dense medium. We show the effects of the chiral condensate and deconfinement phase transition in order to characterize the chiral phase structure of many hadrons. The PNJL model is limited to study (pseudo)scalar meson states. Only pseudoscalar and vector meson masses are available in the lattice QCD calculations of the HotQCD Collaboration [30] and PACS-CS Collaboration [31].

The estimation of the meson masses seems to agree well with Refs. [23,24,38,70]. But for mixing strange with nonstrange scalar states, one state <1 GeV and another one >1 GeV were obtained in Ref. [38]. To this end the authors needed to implement Gyuri fit to correct this [56].

1. *Temperature dependence*

In the presence of chiral symmetry breaking and the correction of the Polyakov-loop potential, we present different scalar and vector meson nonets in thermal and hadronic dense medium and estimate the corresponding meson spectrum. We start with meson masses at finite temperature and varying baryon chemical potential in both LSM and PLSM. The thermal evolutions for scalars and pseudoscalars are shown in Figs. 5 and 6, respectively. The vector and axial-vector results are presented in Fig. 7. In the same way, the mass spectrum at nonzero chemical potential in both LSM and PLSM in dense medium are shown in Figs. 8 and 9 for scalar and pseudoscalar mesons and in Fig. 10 for both vector and axial-vector mesons.

The temperature variations of mesonic masses can be understood as the in-medium thermal effects on the mesonic states.

TABLE II. A comparison between (pseudo)scalar and (axial-)vector meson sectors in PLSM (present work) and the corresponding results from PNJL [27]. Both are compared with the experimental measurements, PDG [33] and the lattice QCD simulations [30,31].

Sector	Symbol	PDG [33]	PLSM	PNJL [26,27]	Lattice QCD	
					HotQCD[30]	PACS-CS [31]
Scalar $J^{PC}=0^{++}$	a_0	$a_0(980^{\pm 20})$	1026	837		
	κ	$K_0^*(1425^{\pm 50})$	1115	1013		
	σ	$\sigma(400-1200)$	800	700		
	f_0	$f_0(1200-1500)$	1284	1169		
Pseudoscalar $J^{PC}=0^{-+}$	π	$\pi^0(134.97^{\pm 6.9})$	120	126	$134^{\pm 6}$	$135.4^{\pm 6.2}$
	K	$K^0(497.614^{\pm 24.8})$	509	490	$422.6^{\pm 11.3}$	$498^{\pm 22}$
	η	$\eta(547.853^{\pm 27.4})$	553	505	$579^{\pm 7.3}$	$688^{\pm 32}$
	η'	$\eta'(957.78^{\pm 60})$	965	949		
Vector $J^{PC}=1^{-}$	ρ	$\rho(775.49^{\pm 38.8})$	745		$756.2^{\pm 36}$	$597^{\pm 86}$
	ω_x	$\omega(782.65^{\pm 44.7})$	745		$884^{\pm 18}$	$861^{\pm 23}$
	K^*	$K^*(891.66^{\pm 26})$	894		$1005^{\pm 93}$	$1010.2^{\pm 77}$
	ω_y	$\phi(1019.455^{\pm 51})$	1005			
Axial vector $J^{PC}=1^{++}$	a_1	$a_1(1030-1260)$	980			
	f_{1x}	$f_1(1281^{\pm 60})$	980			
	K_1^*	$K_1^*(1270^{\pm 7})$	1135			
	f_{1y}	$f_1(1420^{\pm 71.3})$	1315			

As shown in Figs. 5 and 6, respectively, the bosonic thermal contributions to the mesonic masses decrease with increasing temperature, while the fermionic contributions increase at high temperatures. The fermionic (quark) contributions are negligible at small temperatures. At high temperatures, the bosonic thermal contributions dominate. This leads to degeneration in the mesonic masses, which in turn leads to a natural change in chiral and deconfinement phase transition with increasing temperature.

In Fig. 5, the left-hand panel shows the two scalar meson sectors, a_0 and σ, and the two pseudoscalar meson sectors, η' and π, in thermal hadronic medium at vanishing baryon chemical potentials μ in the presence of $U(1)_A$ symmetry breaking. The $U(1)_A$ symmetry breaking gets effectively restored and repeals the mass gap between the chiral partners [23], where at very large temperatures comparable to the strange quark mass, the difference between the strange and nonstrange mesons becomes negligible; see Fig. 2. Accordingly, all mesonic masses will degenerate. Since at very high temperature the major effect takes place in the strange masses, such as a_0 and η', the masses of σ and π degenerate in close vicinity of reduced temperature. This result is compatible with the result reported in Ref. [23]. The masses of a_0 and η' $\sim$250 MeV and masses of σ and π $\sim$181 MeV. The term with $U(1)_A$ symmetry breaking appears in the meson masses through the anomaly breaking term, c. It is strongly related to the strange condensate σ_y. In the right-hand panel, the Polyakov-loop correction is introduced. This correction seems to enhance the quark dynamics and raise the mass degeneration in a sharp and fast way.

In Fig. 5, the different panels present a systematic study of the effects of the chemical potentials on the sixteen mesonic states. We find that increasing the baryon chemical potential (from top to bottom panels) enhances the degeneration of the mesonic masses. For example, at $\mu = 100$ MeV, four meson states a_0 and η' become degenerate at $\sim$240 MeV, σ and π at $\sim$180, while at $\mu = 220$ MeV the four states a_0 and η' degenerate at $\sim$170 MeV, σ and π at $\sim$125 MeV. This has a close relationship with the chiral condensate and the deconfinement phase-transition. In Fig. 3, the chiral condensates $\bar{\sigma}_x$ and $\bar{\sigma}_y$ and deconfinement phase-transition ϕ and ϕ^* vary with T and μ. The contributions from the nonstrange quarks to the rapid crossover in the nonstrange sector are different and affect the contributions of the mesonic masses very strongly [23].

Figure 6 presents the thermal evolution of the scalars f_0 (horizontal dashed curve) and κ (vertical dashed curve) and pseudoscalars η (dotted curve) and K (solid curve) at different baryon chemical potentials $\mu = 0$, 100, 180, 220, and 300 MeV. We find that the masses of these states degenerate at $T \sim 240$ MeV, especially in LSM. In the same way as shown in Fig. 5 for example, at $\mu = 100$ MeV, the temperatures at which the three mesonic states κ, K, and η become degenerate $T \sim 240$. The strength of the stability state at low temperatures delays as the density increases.

The left-hand panel of Fig. 7 gives the thermal evolution of ρ, ω, a_1, f_1, κ^*, K^*, and ϕ calculated in the LSM. We find that the masses of these states degenerate at $T \sim 200$ MeV, while κ^*, K^*, and ϕ degenerate at $T \sim 240$ MeV. At high temperatures, it is obvious that the effects of the nonstrange mass vanish. This makes the differences between the various masses disappear. Increasing the baryon chemical potential reduces the temperatures at which the masses degenerate. This can be understood on the basis of the thermal evolution of

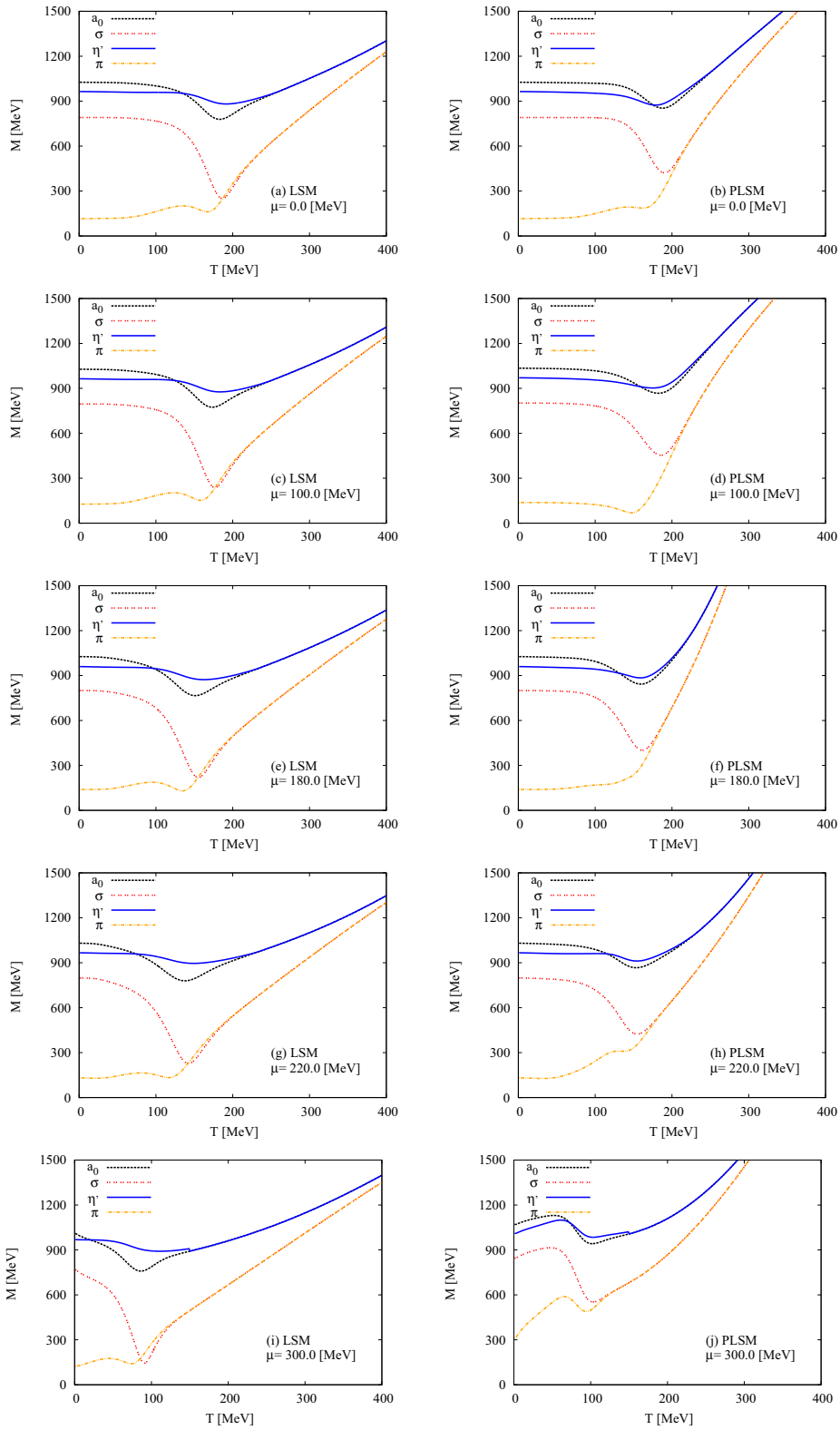

FIG. 5. (Color online) Scalar a_0 (dashed curve) and σ (dotted curve) and pseudoscalar states η' (solid curve) and π (dashed-dotted curve) are given as function of temperature at different baryon-chemical potentials $\mu = 0$, 100, 180, 220, and 300 MeV. The left-hand panel shows LSM results. The PLSM results are presented in the right-hand panel.

the chiral condensates and the deconfinement phase transition, shown in Fig. 3. At $\mu = 300$ MeV, ρ, ω, a_1, and f_1 degenerate at $T \sim 110$ MeV, while κ^*, K^*, and ϕ degenerate at $T \sim 140$ MeV. The right-hand panel presents the same results but calculated in PLSM. The Polyakov-loop correction causes a sharp and fast mass-degeneration.

The mass degeneration can be interpreted as an effect of the fermionic vacuum fluctuations on the chiral symmetry restoration [23], especially on the condensate σ_y. The effect seems to melt the strange condensate faster than the nonstrange one σ_x; see Fig. 1. At very high temperature, the mass gap between mesons seems to disappear and decrease with the

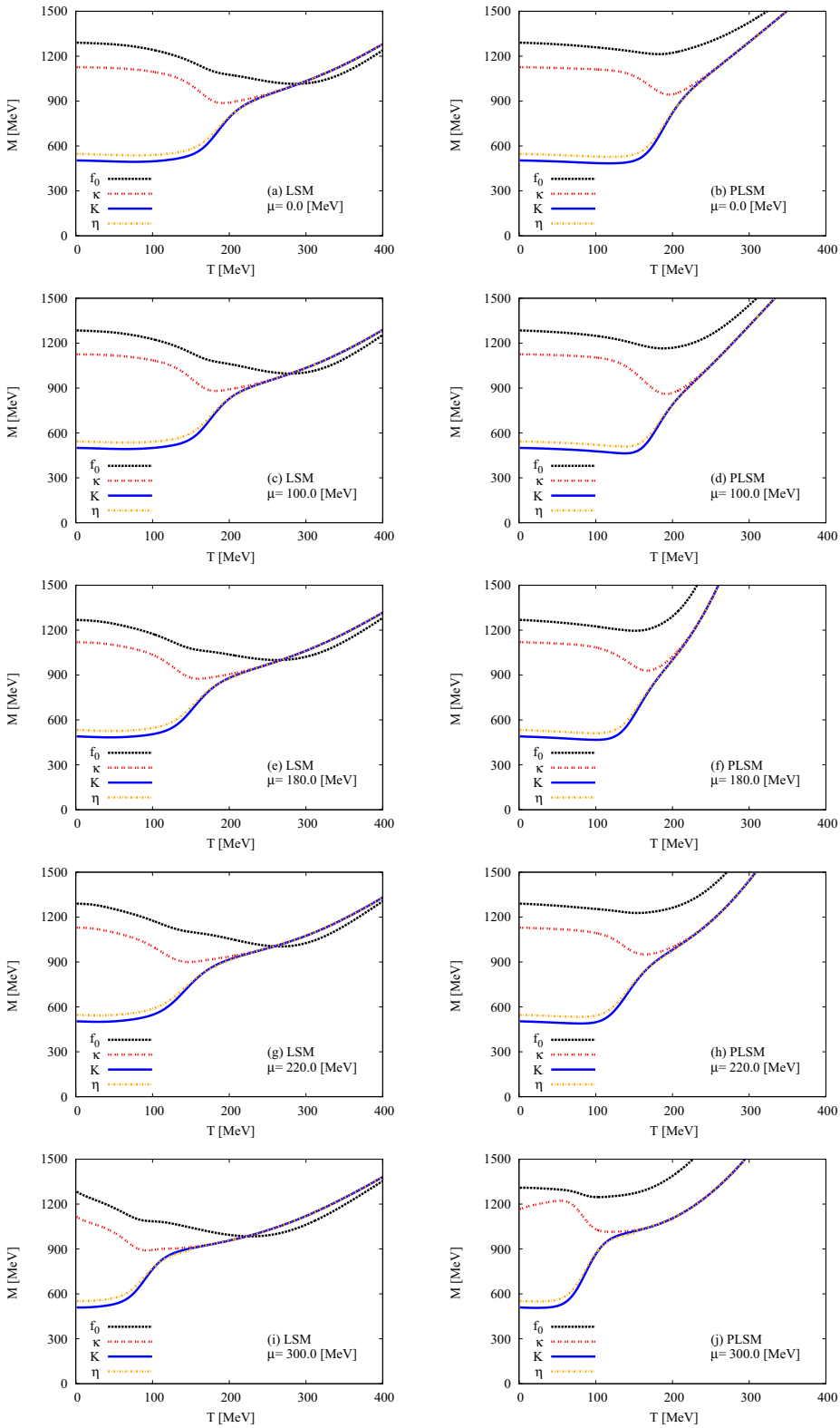

FIG. 6. (Color online) Left-hand panel (LSM) and right-hand panel (PLSM): scalars f_0 (horizontal dashed curve) and κ (vertical dashed curve) and pseudoscalars η (dotted curve) and K (solid curve) are given in dependence on the temperature at different baryon chemical potentials $\mu = 0$, 100, 180, 220, and 300 MeV.

melting strange condensate σ_y. This mass gap appears at low temperatures, where the nonstrange condensate remains finite. At temperatures higher than the critical value only the strange condensate remains finite. This thermal effect is strongly related to the degeneration of the meson masses.

2. Density dependence

The meson masses are shown for the case with $U(1)_A$ anomaly as a function of baryon chemical potential at different temperatures in the LSM (left-hand panel) and the PLSM (right-hand panel), where the scalar and pseudoscalar are

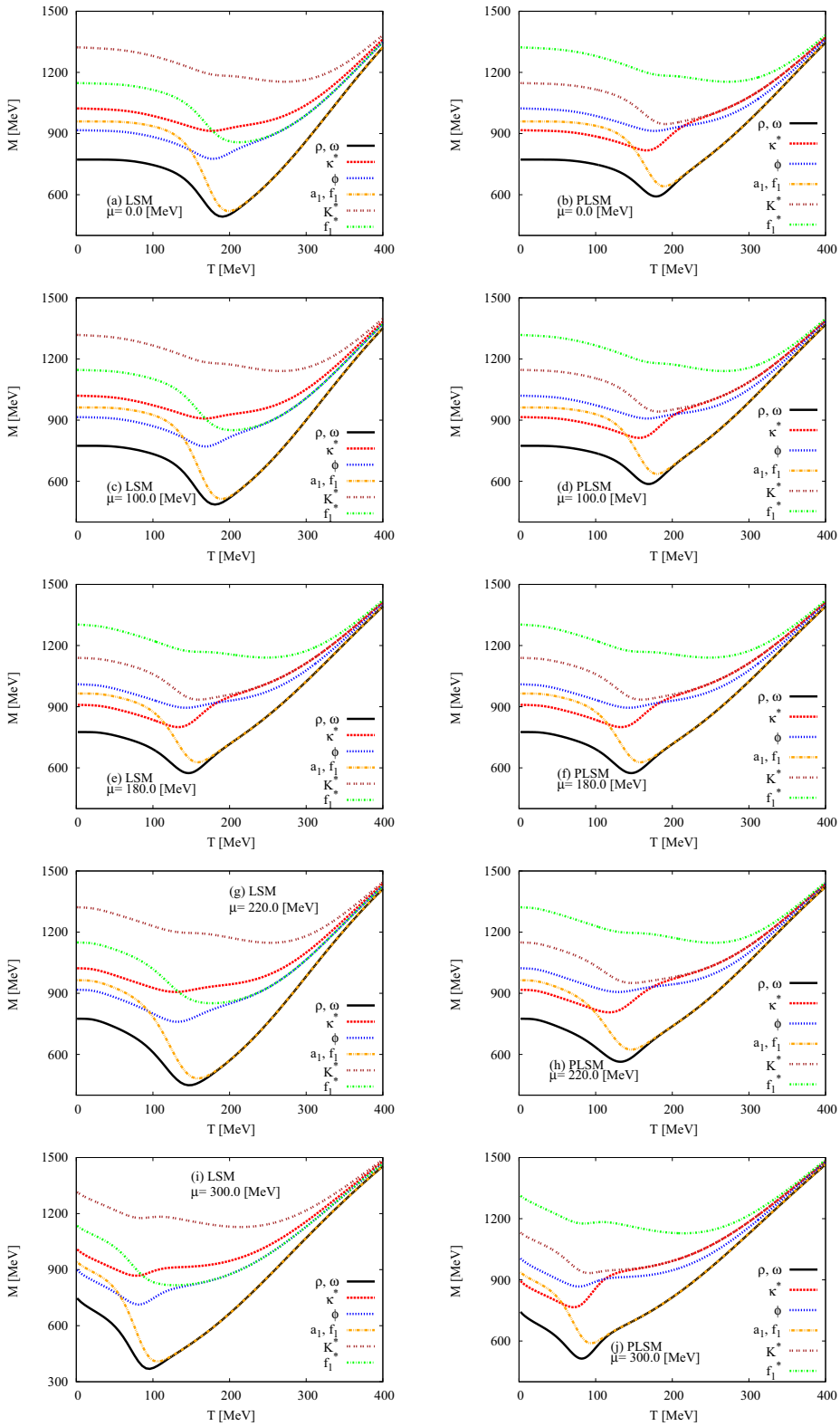

FIG. 7. (Color online) Left-hand panel (LSM) and right-hand panel (PLSM): vector mesons ρ and ω (solid curve), κ^* (long-dotted curve) and ϕ (dotted curve) and axial-vector mesons $a_1 = f_1$ (dashed-dotted curve), K^* (dotted curve), and f_1^* (short-dashed-dotted curve) are given in T dependence at different baryon-chemical potentials $\mu = 0$, 100, 180, 220, and 300 MeV.

presented in Figs. 8 and 9 while the vector and axial-vector mesons are depicted in Fig. 10.

In left-hand panel of Fig. 8, we notice that all masses keep their vacuum values almost unchanged until the baryon chemical potential reaches the Fermi surface for the light quarks [72] at $\mu \sim 350$ MeV. The mass of the σ meson drops below the mass of the π meson at the value where the first-order transition should be positioned [72]. This means that the masses of pseudoscalar mesons stay nearly constant until the phase transition takes place, Fig. 8, while the scalar mesons show a stronger melting behavior above the Fermi surface for the light quarks [72]. The right-hand panel presents

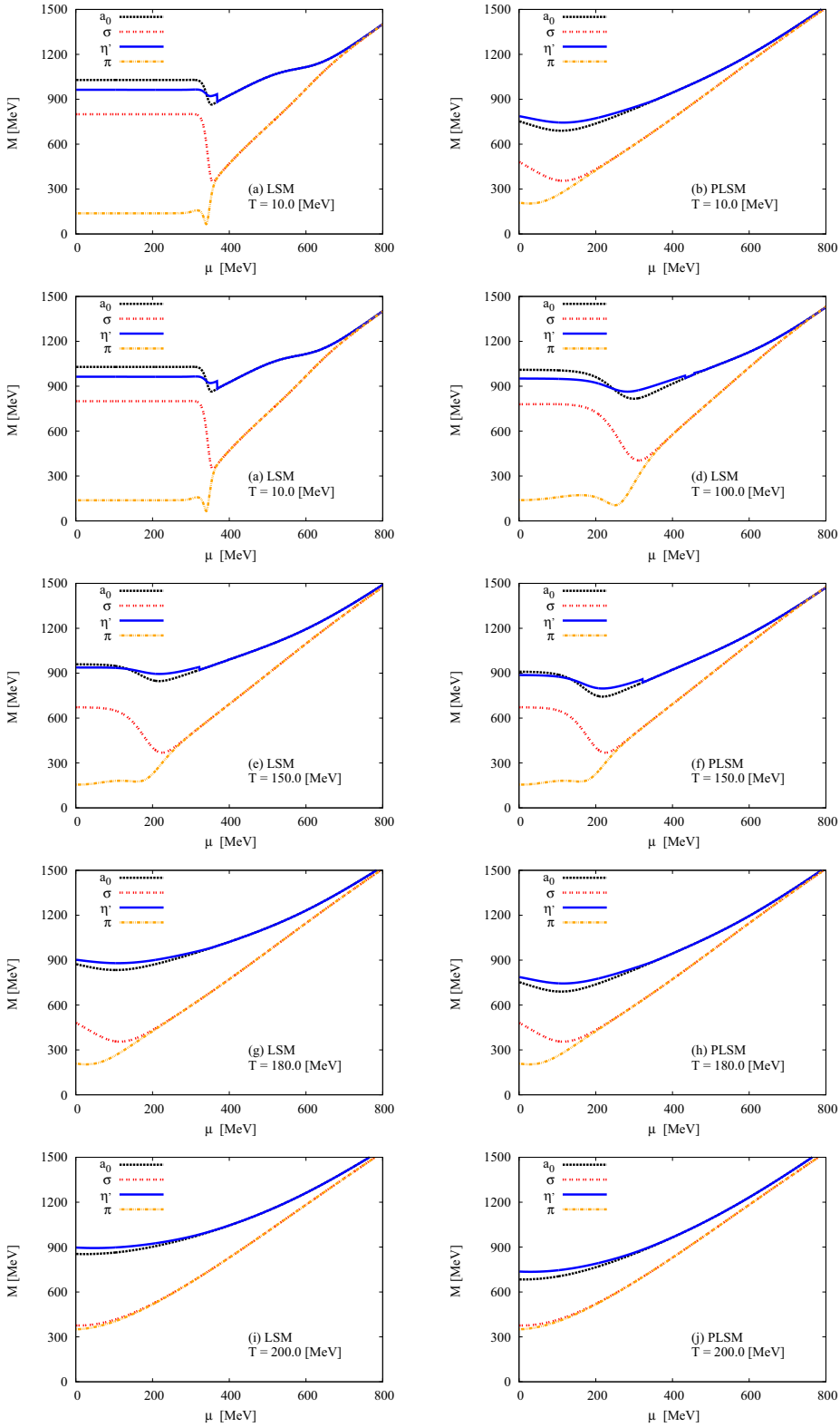

FIG. 8. (Color online) Left-hand panel (LSM) and right-hand panel (PLSM) present scalars a_0 (dashed curve) and σ (dotted curve) and pseudoscalars η' (solid curve) and π (dashed-dotted curve) in hadronic dense medium at fixed temperatures $T = 10$, 100, 150, 180, and 200 MeV.

the effects of the Polyakov-loop correction introduced to the quark dynamics. This causes a sharp transition in the mass degeneration. The increase of the melting behavior above T_c derives the masses to be compacted with each other.

In left-hand panel of Fig. 9, we find again that all masses stay at their vacuum values until the baryon chemical potential reaches the Fermi surface for the light quarks at $\mu \sim 350$ MeV. The meson masses drop at the first-order transition and the κ meson drops below the masses of K and η mesons. Only in the curve for the f_0 meson is the Fermi surface for the strange quarks clearly visible. The mass of f_0 decreases below κ. Masses of K and η decrease only after the light quark phase

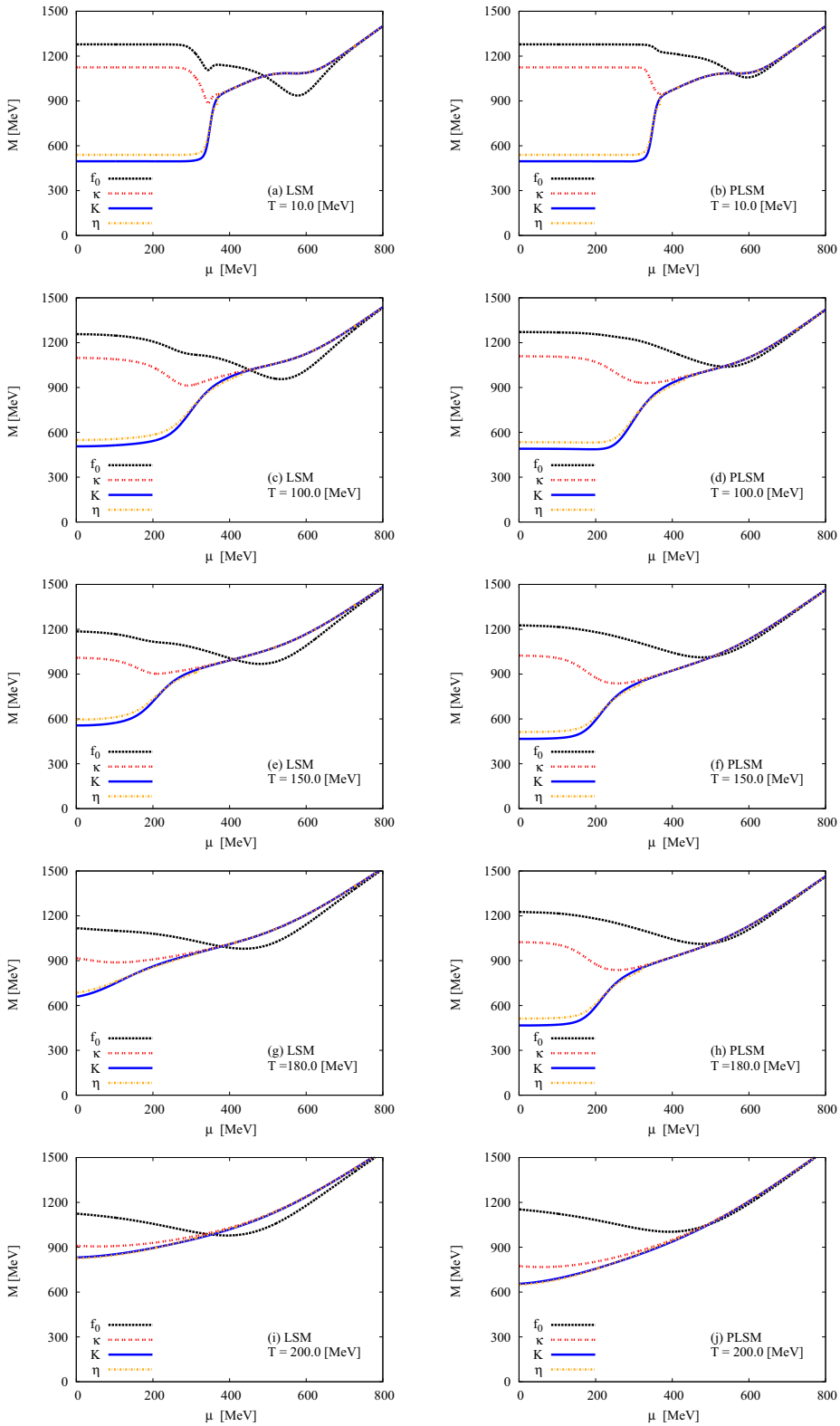

FIG. 9. (Color online) Left-hand panel (LSM) and right-hand panel (PLSM) show scalars f_0 (horizontal dashed curve) and κ (vertical dashed curve) and pseudoscalars η (dotted curve) and K (solid curve) in hadronic dense medium at fixed temperatures $T = 10$, 100, 150, 180, and 200 MeV.

transition (this the second phase transition) and degenerate with other meson masses at very high chemical potential $\mu = 700$ MeV. This value decreases as the melting point of the system increases. The first slight drop of the f_0 meson takes place at $\mu \sim 350$ MeV, due to the induced drop in the strange condensate. The right-hand panel shows that the Polyakov-loop correction introduces quark dynamics. Apparently, this enhances the mass degeneration through the deconfinement phase transition to appear sharper and faster than in the LSM.

Figure 10 shows the LSM (left-hand panel) and PLSM (right-hand panel) results of vector and axial-vector mesons as a function of the baryon chemical potentials at different fixed

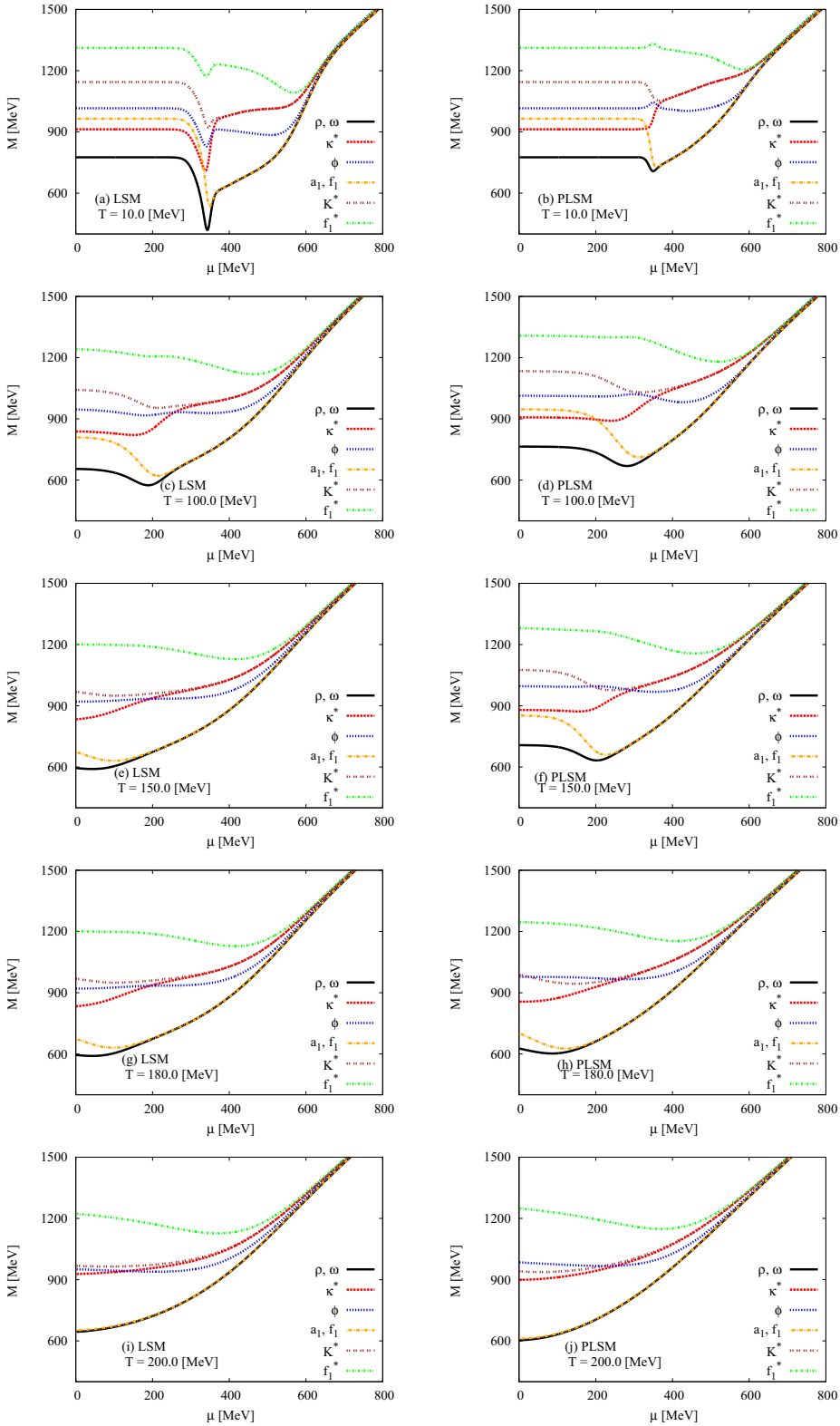

FIG. 10. (Color online) The left-hand panel (LSM) and right-hand panel (PLSM) show vector mesons ρ,ω (solid curve), κ^* (long-dotted curve), and ϕ (dotted curve) and axial-vector mesons $a_1 = f_1$ (dashed-dotted curve), K^* (dotted curve), and f_1^* (short-dashed-dotted curve) in hadronic dense medium at different temperatures $T = 10$, 100, 150, 180, and 200 MeV.

temperatures. This gives a systematic study for the variation of heating effect on the hadronic dense medium. In the left-hand panel we find that the axial-vector mesons a_1 and f_1 keep their vacuum values till $\mu = 350$ MeV. Then, they drop below the values of vector mesons ρ and ω. This is accompanied by a strong phase transition (first order) and a degeneration in the masses. The axial-vector meson K^* keeps its vacuum value till the same value of the baryon chemical potential. Then, it drops below the values of vector mesons ρ and ω. In this case, this is accompanied by a rapid phase transition (first order). The strange meson states f_1^* and ϕ degenerate only at very high chemical potential, $\mu \sim 700$ MeV. These μ values decrease

with increasing T. Increasing T reduces the baryon chemical potential, at which the mass degeneration gets compatible with the previous cases and easily gaps the Fermi surface for the light quarks. These would mean that the masses of vector mesons stay nearly constant until the phase transition takes place, while the masses of the axial-vector mesons show a stronger melting above the Fermi surface for the light quarks.

The right-hand panel Fig. 10 shows the in-medium effect of the baryon chemical potential (density) on the vector and axial-vector mesons in the presence of Polyakov-loop correction and symmetry breaking. We find that the deconfinement phase transition has considerable effects on the chiral phase transition in meson masses, where the restoration of the chiral symmetry breaking becomes sharper and faster than in the LSM. For example, very close to the critical temperature, $T = 180$ MeV, the axial-vector mesons a_1 and f_1 keep their vacuum values till $\mu \sim 180$ MeV. Then, the two masses become smaller than that of the vector mesons ρ and ω. The axial-vector meson, K^*, keeps its vacuum value till $\mu \sim 300$ MeV. Then, its mass drops below the ones of the vector mesons ρ and ω. At a characteristic value of the baryon chemical potential, the masses of all mesons degenerate with each other.

B. Exclusion of anomalous terms

The axial anomalous term $U(1)_A$ is considered by an effective 't Hooft determinant in the Lagrangian, which breaks $U(1)_A$ symmetry [4,73]. This term appears in the anomaly Lagrangian, Eq. (5), and in the pure mesonic potential, Eq. (26), through the parameter c. Eliminating this term likely affects the chiral phase transition and plays an essential role onin the phenomenology of scalar and pseudoscalar masses at finite temperature and density. The vector and axial-vector masses are not affected by the anomalous term; see Eqs. (38)–(45). It is conjectured that the axial anomaly-breaking term is constant (not depending on temperature and chemical potential) [23]. In this section, we introduce the influence of the axial anomaly on the meson masses.

In the case that the anomalous terms depend on the temperature, a fast effective restoration of the axial symmetry takes place [23]. It was found that the anomalous term decreases with increasing temperature [23]. At very high temperatures, both chiral condensates σ_x and σ_y degenerate [23].

In the case that the chiral condensates depend on the baryon chemical potential, we find that the upper Fermi surface of the light quarks coincides with the light quark mass, $\mu \approx m_l = 300$ MeV, where the chiral condensates are in the broken phase (below the phase transition) and the strange condensate has no influence on the axial anomaly [23]. The phase transition is mainly estimated by the nonstrange condensate σ_x, while the leap in the strange condensate σ_y can be neglected. Below the Fermi surface (above the phase transition), the strange condensate should be taken into account: $\mu \approx m_g = 433$ MeV.

1. Temperature dependence

The thermal evolution of the meson states in the case of negligible influence of the axial anomaly term $U(1)_A$ at vanishing baryon chemical potential $\mu = 0.0$ MeV, LSM (left-hand panel) and PLSM (right-hand panel), in Fig. 11, shows that the critical temperature T_c remains unchanged, the mass gap between the chiral partners vanishes in the restored phase, and all meson states begin to degenerate at the chiral restoration temperature T_c^q of light quarks. This value of T_c^q does not change when introducing the anomaly term. The introduction of color and gluon dynamics in form of Polyakov-loop corrections to a_0 and σ. Both drop to η' and π.

Figure 12 shows that the chiral restoration remains incomplete till the temperature exceeds the critical one corresponding to the chiral restoration for light quarks. In the presence of an axial anomaly term, it is obvious that the four meson states degenerate at the same approximative temperature. The chiral restoration for strange quarks is not fully completed because η degenerates with κ and K at values larger than that of the chiral restoration of the light quarks, T_c^q. These values are not changed in both cases, i.e., with/without anomaly. But they increase when introducing color and gluon interaction.

2. Density dependence

The density evolution of mesonic states in the case of negligible influence of the axial anomaly term $U(1)_A$ at finite temperate is evaluated at $T = 10$ MeV in LSM (left-hand panel)

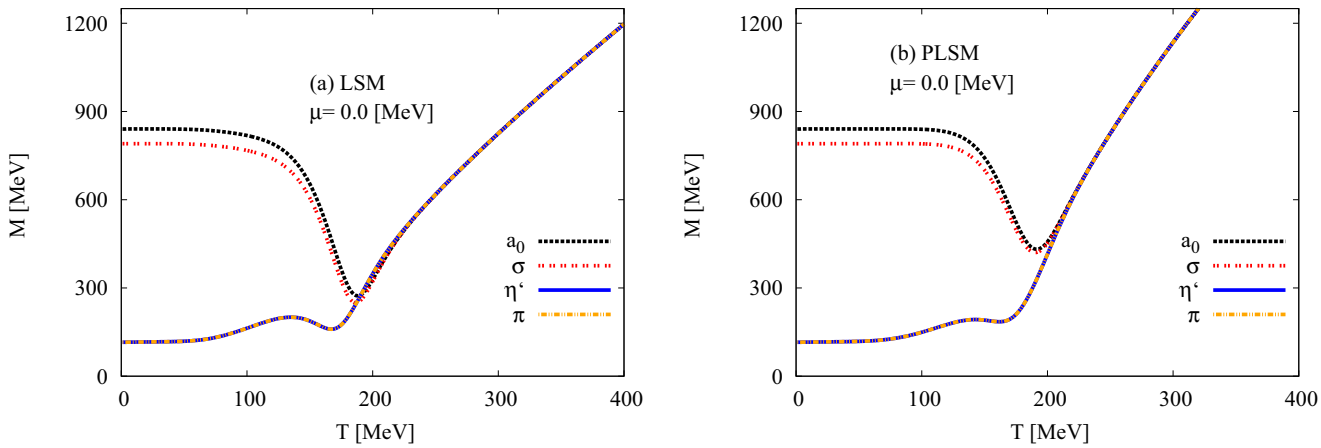

FIG. 11. (Color online) Left- (LSM) and right-hand panels (PLSM) show scalar a_0 (dashed curve) and σ (dotted curve) and pseudoscalar states η' (solid curve) and π (dashed-dotted curve) as a function of temperature at vanishing baryon chemical potentials $\mu = 0.0$ MeV.

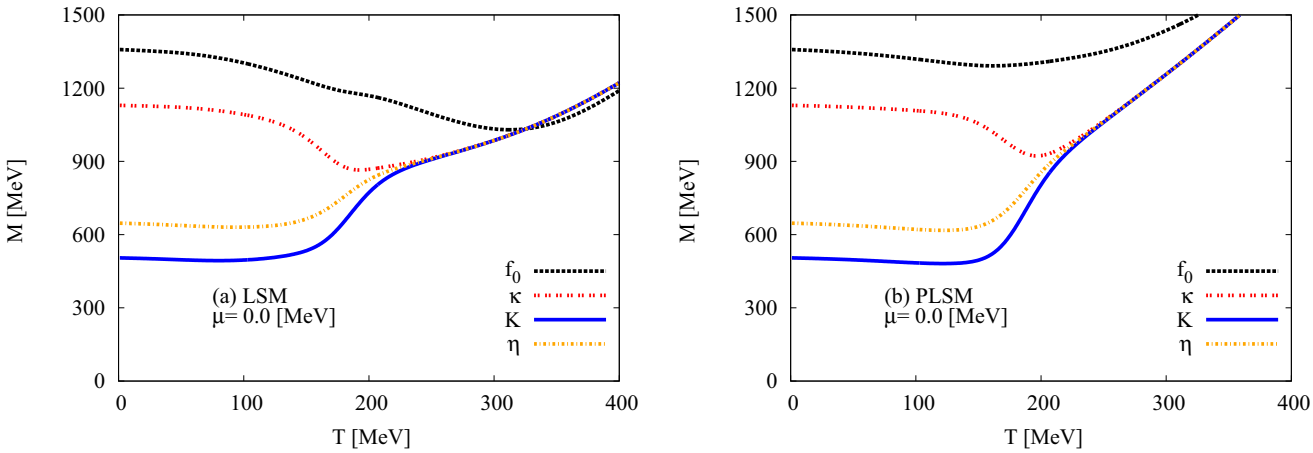

FIG. 12. (Color online) Left- (LSM) and right-hand panels (PLSM) show scalars f_0 (horizontal dashed curve) and κ (vertical dashed curve) and pseudoscalars η (dotted curve) and K (solid curve) as a function of temperature at vanishing baryon chemical potentials $\mu = 0.0$ MeV.

and PLSM (right-hand panel) in Fig. 13. The critical temperature does not change from the case in which the axial anomaly term is included. But the introduction of the color dynamics in the absence of the axial anomaly term appears in the left-hand panel of Fig. 13. The limit of the Fermi surface is unchanged in both cases, i.e., with and without anomaly. In Fig. 13, the drops of a_0 and σ states to η' and π states are slow. This is sharp and localized in a small region around the critical μ_c. The phase transition is first order. This means that the scalar mesons show a stronger melting behavior, while the introduction of the color dynamics of quarks bears out the pseudoscalar states to have a large melting point as shown in the left-hand panel of Fig. 13. The degenerate states between all four meson masses are assumed to take place at second-order phase transition.

In Fig. 14, the κ state drops to the K and η states in a first-order phasetransition, but the chiral phase restoration will not be completed till f_0 degenerates at a higher-order phase transition. All properties obtained in the case of including an anomaly are also observed in the case without anomalous terms.

C. Numerical parameters of the model

Table IV summarizes the numerical values of the various parameters of the present work. These have be deduced from the thermal and density evolution of the scalar and pseudoscalar meson masses [23]. Here, we distinguish between the cases where the anomalous terms, c, are finite and vanishing.

Table V summarizes the numerical values of the various parameters of the model used in this work. They have been deduced from the thermal and density evolution of the vector and axial-vector meson masses [23].

V. NORMALIZATION TO LOWEST MATSUBARA FREQUENCY

In finite temperature field theory, the Matsubara frequencies are a summation over the discrete imaginary frequency, $S_\eta = T\sum_{i\omega_n} g(i\omega_n)$, where $g(i\omega_n)$ is a rational function, $\omega_n = 2n\pi T$ for bosons, and $\omega_n = (2n+1)\pi T$ for fermions and $n = 0, \pm1, \pm2, \ldots$ is an integer (plays the role of a quantum number). By using Matsubara weighting function

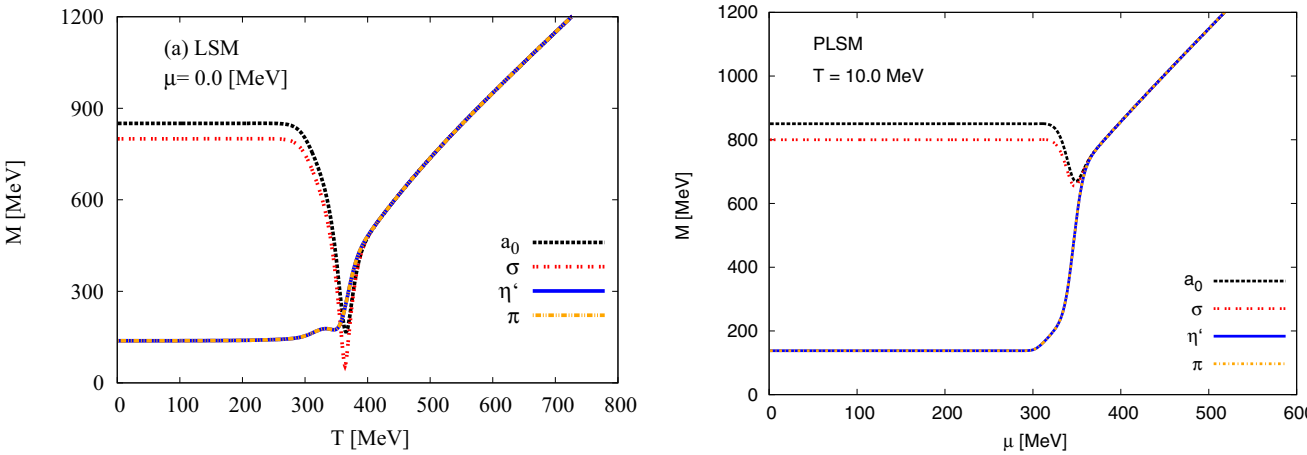

FIG. 13. (Color online) Left- (LSM) and right-hand panels (PLSM) present scalars a_0 (dashed curve) and σ (dotted curve) and pseudoscalars η' (solid curve) and π (dashed-dotted curve) in dense medium at fixed temperature $T = 10$ MeV.

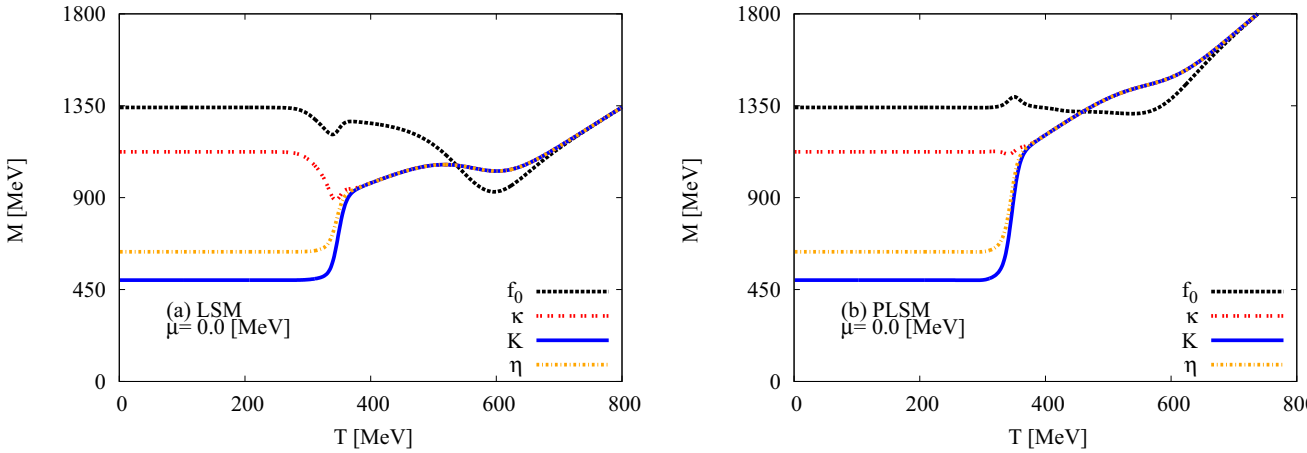

FIG. 14. (Color online) Left- (LSM) and right-hand panels (PLSM) show scalars f_0 (horizontal dashed curve) and κ (vertical dashed curve) and pseudoscalars η (dotted curve) and K (solid curve) in dense medium at fixed temperature $T = 10$ MeV.

$h_\eta(z)$, which has simple poles exactly located at $z = i\omega_n$, then

$$S_\eta = \frac{T}{2\pi i}\oint g(z)\, h_\eta(z)\, dz, \tag{53}$$

where $\eta = \pm$ stands for the statistic sign for bosons and fermions, respectively. $h_\eta(z)$ can be chosen depending on which half-plane the convergence is to be controlled,

$$h_\eta(z) = \begin{cases} \eta\frac{1+n_\eta(z)}{T}, \\ \eta\frac{n_\eta(z)}{T}, \end{cases} \tag{54}$$

where $n_\eta(z) = (1 + \eta e^{z/T})^{-1}$ is the single-particle distribution function.

The mesonic masses are conjectured to have contributions from the Matsubara frequencies [74]. Furthermore, at high temperatures ($\geqslant T_c$), the behavior of the thermodynamics quantities, including the quark susceptibilities, besides the masses, is affected by the interplay between the lowest Matsubara frequency and the Polyakov-loop correction [75]. We apply normalization for the different mesonic sectors with respect to the lowest Matsubara frequency [76] in order to characterize the dissolving temperature of the mesonic bound states. It is found that the different mesonic states have different dissolving temperatures. This would mean that the different mesonic states have different T_c's, at which the bound mesons begin to dissolve into quarks. Therefore, the masses of different meson states should not be different at $T > T_c$. To a large extend, their thermal and density dependence should be removed, so that the remaining effects are defined by the free energy [74], i.e., the masses of *free* bosons are defined by m_l.

That the masses of almost all mesonic states become independent of T, i.e., constructing a kind of a universal line, would be seen as a signature for meson dissociation into quarks. It is a deconfinement phase transition, where the quarks behave almost freely. In other words, the characteristic temperature should not be universal, as well. So far, we conclude that the universal T_c characterizing the QCD phase boundary is indeed an approximative average (over various bound states).

A. Critical temperatures and critical chemical potentials

In left-hand panel of Fig. 15, it is obvious that each scalar and pseudoscalar meson normalized to the lowest Matsubara frequency begins to dissolve into its quark constituents, individually. At very high temperatures, we expect a universal line independent of temperature, where many bound particles dissolve entirely. For example, κ, K, a_0, η, η', f_0, σ, and π dissolve slowly. The right-hand panel shows the same behavior but corresponding to vector and axial-vector mesons, where ρ, ω, a_1, f_1 dissolve rapidly, while f_1^* is the last bound state, which seems to survive the typical T_c. In Table III, different meson states are listed corresponding to their dissolving temperatures.

In Fig. 16, the top panels show the in-medium effects of the baryon-chemical potential (density) on the masses of mesonic states normalized to the lowest Matsubara frequency at a fixed temperature lower than the typical T_c. It is obvious that increasing μ also brings the masses very close to a universal value, i.e., free energy. The bottom panels show the same but at a fixed temperature higher than the typical T_c.

TABLE III. The approximative dissolving temperature corresponding to the different meson states.

Meson	Scalar mesons				Pseudoscalar mesons				Vector mesons				Axial-vector mesons			
	a_0	κ	σ	f_0	π	K	η	η'	ρ	K_0^*	ω	ϕ	a_1	K_1	f_1	f_1^*
$T_{\text{dissolving}}^{\text{Meson}}$ (MeV)	200	250	320	320	320	230	235	300	195	300	195	300	205	250	205	350

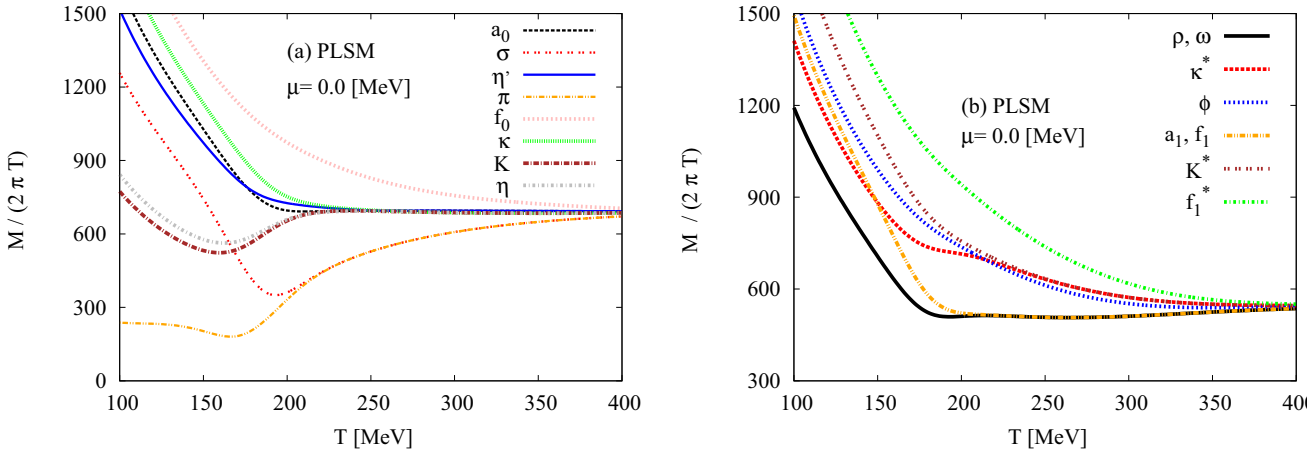

FIG. 15. (Color online) The left-hand panel shows scalar and pseudoscalar meson sectors in thermal medium at vanishing baryon chemical potential, while the right-hand panel refers to the vector and axial-vector meson sectors.

Here, increasing μ seems to bring the masses very close to a universal value in a faster and easier way. Finally, it is apparent that the temperature (an essential quantity in the lowest Matsubara frequency) should be corrected or weighted in order for the matrix model to reproduce the mean field results correctly [75].

VI. MESON MASSES IN THE LARGE-N_c LIMIT

When replacing the QCD gauge symmetry SU(3) by SU(N_c), where $N_c \gg 3$ is the number of colors, we obtain a simpler QCD theory. In other words, such a large-N_c limit offers an effective approach to study QCD [77]. The relevant quantities can be given in N_c^{-n} series, so that large-N_c dominance can be separated from suppressed terms. In doing this and in order to guarantee a consistent large-N_c approach, the QCD coupling g_{QCD} must be scaled [78]; $g_{QCD}\, N_c \to$ finite, if $N_c \to \infty$. Accordingly, it was concluded in Ref. [78] that the meson masses scale with N_c while the interaction scales with $N_c^{-(k-2)/2}$. The decay amplitudes are suppressed as $1/\sqrt{N_c}$ [78]. In this limit, the meson masses will be stable and noninteracting. At finite T, a noninteracting gas of mesons is realized for $N_c \gg 3$.

In defining the quarkyonic phase [79] which is conjectured to separate the hadronic from the partonic phases in the $T-\mu$ phase diagram, the large-N_c approach has been implemented [80]. Accordingly, the limits for the chiral models should be corrected for low-energy hadrons (having densities close to that of the nuclear matter) [79]. At very low temperatures, this should agree with the Walecka limit [81]. The properties of nuclear matter and chiral phase transition have been investigated in the large-N_c limit [77,79]. There is only one case in which nuclear matter does not disappear by increasing N_c. This is the naive quarkonium assigned to the lightest scalar resonance [82]. The low-energy hadrons (light scalar states below 1 GeV) do not formulate quarkonium states predominantly. On the other hand, the resulting nucleon-nucleon attraction in the scalar channels is not strong enough to bind nuclei [77,79].

In order to study the behavior of the meson masses with varying N_c, we start with the PLSM normalized chiral condensates, σ_x and σ_y, and the Polyakov-loop fields, ϕ and ϕ^*, at finite temperatures and vanishing baryon chemical potential; see Fig. 17. We find that ϕ and ϕ^* are good indicators for the deconfinement phase transition. Both order parameters possess information about the confining glue sector to the effective chiral model, the LSM. From the quark-antiquark potential, Eqs. (18) and (25), it is obvious that the Polyakov-loop expectation values vary with N_c. We expect that the deconfinement phase transition moves to higher critical temperatures with increasing N_c and $T_c \to \infty$ when $N_c \to \infty$. Table VI summarizes T_c for light and strange quarks at different N_c.

Figure 18 shows the scalar meson sectors at different N_c as function of T at $\mu = 0$ and $N_c = 3$ (solid curves), $N_c = 6$ (dotted curves), $N_c = 12$ (dashed-dotted curves), and $N_c \to \infty$ (dashed curves). The masses of all mesons are not influenced when varying N_c. It seems that the mesons are stable and noninteracting, especially at densities close to that of nuclear matter. At very low temperatures, the results seem to agree with a Walecka-like model [81]. The meson channels can be divided into three regions; one at low T: one around T_c and one at very high T:

(i) The first region is established where the strong force between quarks should be dominant and the mass

TABLE IV. Scalars and pseudoscalars: the numerical values of the parameters used in the calculations [23].

	c (MeV)	h_x (MeV^3)	h_y (MeV^3)	m^2 (MeV^2)	λ_1	λ_2	g
With anomaly	4807.84	$(120.73)^3$	$(336.41)^3$	$-(306.26)^2$	13.49	46.48	6.5
Without anomaly	0	$(120.73)^3$	$(336.41)^3$	$-(503.55)^2$	−4.55	82.47	6.5

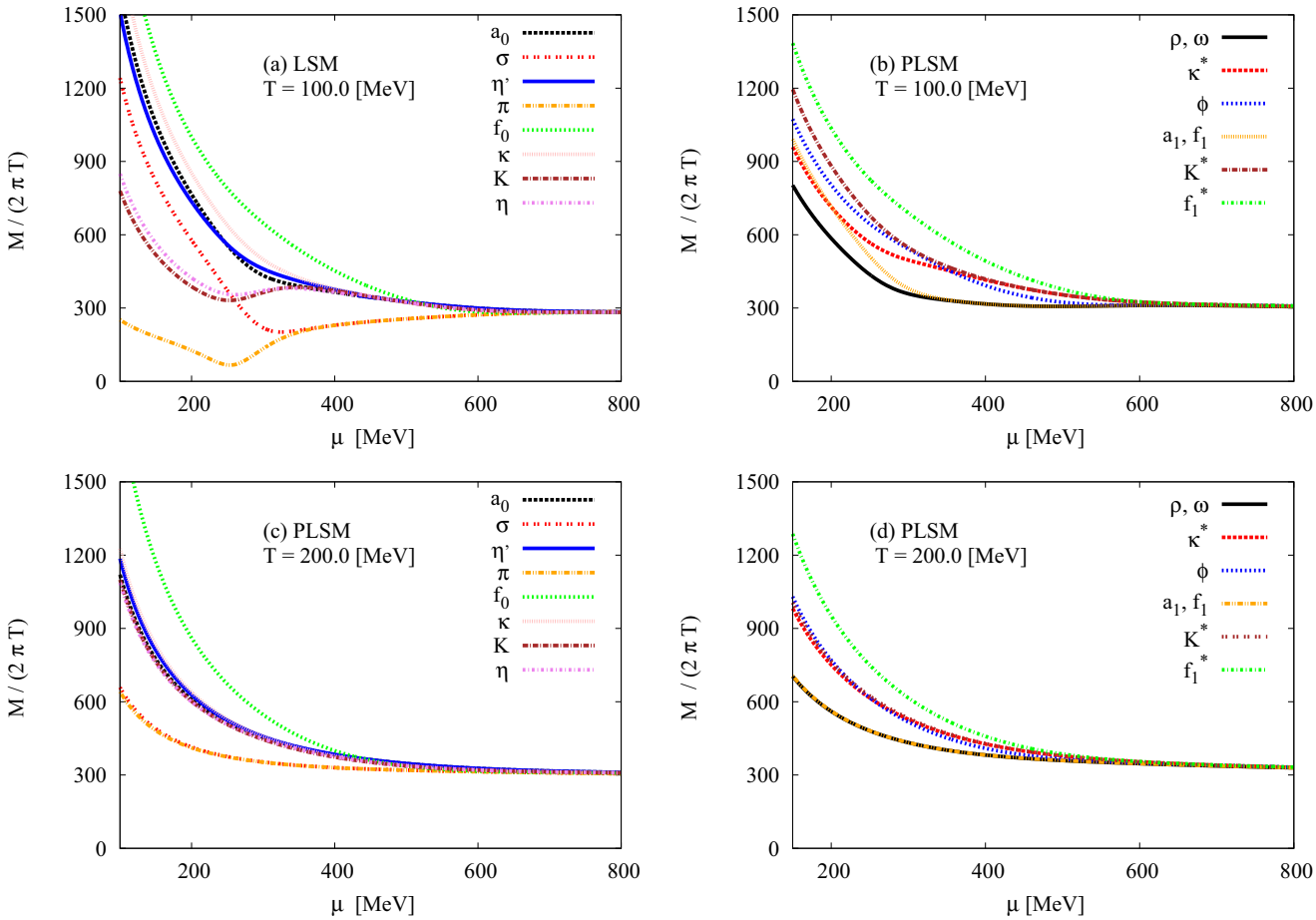

FIG. 16. (Color online) The left-hand panel shows scalar and pseudoscalar mesons at $T < 100$ MeV and at $T > 200$ MeV. The right-hand panel presents vector and axial-vector mesons.

degeneration appears despite of the variation of N_c. This can be interpreted as the effect of the vacuum contributions on the chiral symmetry restoration.

(ii) The second region takes place due to fluctuations in the variation of colors N_c relating to the deconfinement phase transition at T_c.

(iii) In the last region, the bosonic thermal contributions are dominant and the mass gap between mesons seems to disappear. The mesonic states degenerate at large N_c.

In the large-N_c limit, the meson masses are stable and noninteracting at low T. They keep the mass gap between the different meson channels. At high T, this gap disappears and the masses become T independent. Except π and σ, the other scalar meson masses are T independent at large N_c and high T. For the pseudoscalar meson masses, Fig. 19, the large-N_c limit unifies the T dependence of all states in a universal bundle. The same is also observed for axial and axial-vector meson masses in the large-N_c limit; see Fig. 20.

TABLE V. Vectors and axial vectors: the numerical values of the parameters used in the calculations [38].

h_1	h_2	h_3	m_1^2 (MeV^2)	δ_x (MeV^2)	δ_y (MeV^2)	g_1
0	9.87	4.8667	$(0.4135)^2$	0	$(0.1511)^2$	6.5

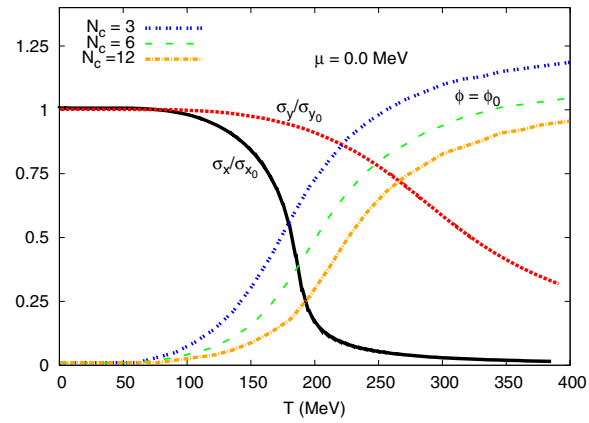

FIG. 17. (Color online) The normalized chiral condensates σ_x and σ_y (solid and dotted curves, respectively) and the expectation values of the Polyakov-loop fields, ϕ and ϕ^* [dotted curve ($N_c = 3$), dashed curve ($N_c = 6$), dotted-dashed curve ($N_c = 12$)], are given as a function of the temperature at vanishing baryon chemical potential.

TABLE VI. Dependence of the critical temperatures for light-quark T_c^l and strange-quark T_c^s on N_c.

N_c	3	6	12
T_c^l [MeV]	181	189	195
T_c^s [MeV]	225	245	270

VII. CONCLUSIONS

There are various approaches implementing theoretical descriptions of the hadron masses in thermal and hadronic dense medium [23–25,44,45]. The NJL (or PNJL) model studies the thermal spectrum of eight mesons: four scalars and four pseudoscalars at vanishing and finite baryon chemical potential [26,27]. Previous works using LSM (or PQM) focused on the study of (pseudo)scalar mesons at finite temperature but vanishing density (baryon chemical potential) [23–25,44,45] and described the vacuum phenomenology of some states in scalar and vector meson nonets, besides the comparison with the experimental measurements for the decay width and the scattering length [36–40].

In the present work, a systematic study using the chiral symmetric linear-σ model is introduced. The scalar, pseudoscalar, vector, and axial-vector fields are included. The representation of all these four categories in dependence on the temperature and on the baryon chemical potential is taken into consideration. This allows us to define the characteristics of the chiral phase structure for all these mesonic states, i.e., in thermal and hadronic dense medium, and determine the critical temperature and density at which each mesonic state breaks into its free quarks.

At vanishing temperature, the scalar, pseudoscalar, vector, and axial-vector meson nonets are compared to the experimental measurements reported by the PDG [33]. Also, we compare the results with the lattice QCD calculations [30,31] for pseudoscalar and vector mesons. The scalar and pseudoscalar

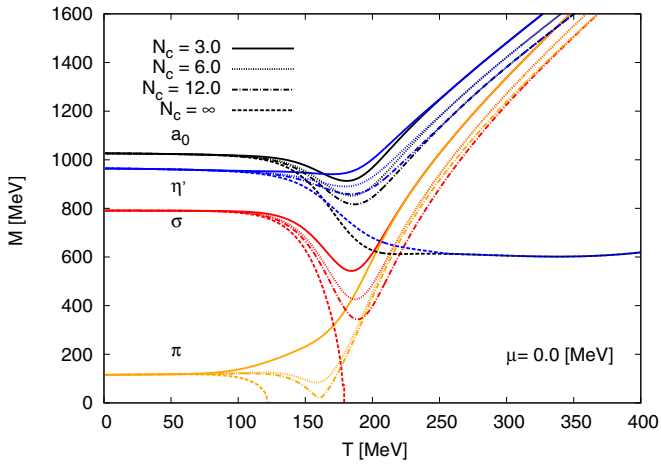

FIG. 18. (Color online) The scalar meson masses are given as a function of T at $\mu = 0$ and $N_c = 3$ (solid curves), $N_c = 6$ (dotted curves), $N_c = 12$ (dashed-dotted curves), and $N_c \to \infty$ (dashed curves).

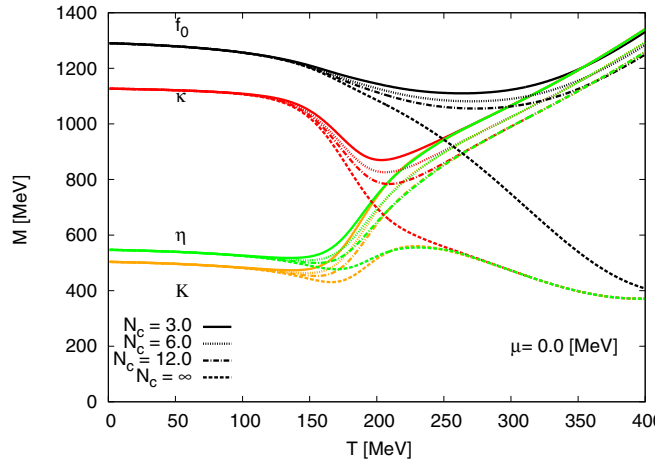

FIG. 19. (Color online) The same as in Fig. 18 but for pseudoscalar meson masses.

spectrum calculated from PNJL [26,27] is compared with the present work, as well. We first want to highlight that the uncertainties are deduced from the fitting for the parameters used in calculating the equation of states and some other thermodynamic quantities. The fitting requires experimental inputs for axial/axial-vector and scalar/pseudoscalar states. Thus, we conclude that the results are very precise for some light hadron resonances. The effects of the chiral condensate and the deconfinement phase transition would play an important role in characterizing the chiral phase structure of many hadrons, and therefore explain the differences seen in the heavy states. The PNJL model is limited to study of (pseudo)scalar meson states. Only pseudoscalar and vector meson masses are available in the lattice QCD calculations of the HotQCD Collaboration [30] and the PACS-CS Collaboration [31]. Relative to these two approaches, it can be concluded that the present work reproduces well the mesonic spectrum.

In order to investigate the influence of the Polyakov-loop potential on the chiral symmetry restoration, the present results are compared with PLSM. The PLSM mainly describes the

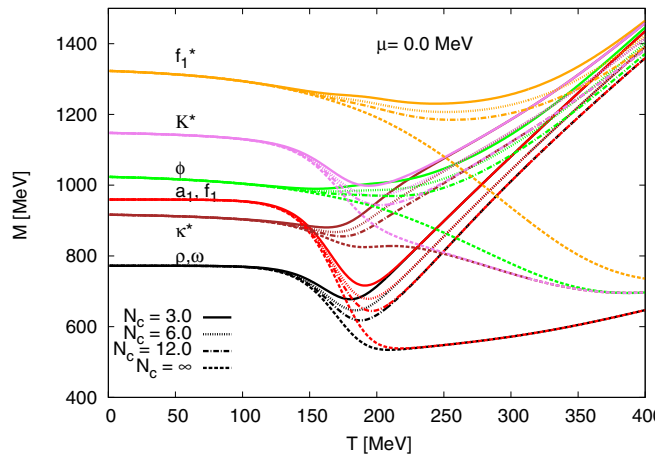

FIG. 20. (Color online) The same as in Fig. 18 but for axial and axial-vector meson masses.

chiral condensates in nonstrange σ_x and strange σ_y condensates in addition to the deconfinement phase transition, ϕ and ϕ^*, in temperature and density (baryon chemical potential) dependence. This allows the estimation of the spectrum of some mesonic states in SU(3) as a result of the chiral phase structure of scalar/pseudoscalar and axial/axialvector states at various densities and temperatures. First, we compare the critical temperatures estimated from at the phase transition and from the order parameters. We found that the chiral phase transition gets shifted to higher temperatures as a result of the inclusion of the Polyakov loop in LSM. In the mesonic masses, the thermal bosonic contributions decrease with increasing temperature, while the fermionic contributions increase at high temperature. At low temperatures, the fermionic contributions are negligible. The early (related to low critical temperature and/or small chemical potential) melting of the strange condensate σ_y relative to the nonstrange one can be interpreted due to the mass degeneration at larger values of temperature and/or chemical potential. In the phase where the symmetry is explicitly broken in PLSM, the meson masses generated by PLSM have a good agreement with the experimental results.

We have illustrated that the PLSM can be used to check which mesonic states degenerate with (an)other one(s) and which states degenerate faster relative to the other ones, especially near the Fermi surface. The limitation that all hadrons should melt at a universal critical temperature (QCD phase boundary) can be understood as an approximation. We conclude that each bound state would have a characteristic temperature and density (baryon chemical potential) at which it dissolves to its free quarks. We plan to extend this study by including more mesonic states and characterizing their thermal and density evolution. Also, we want to introduce some low-lying baryonic states. Such a plan requires a basic modification of the Lagrangian. The normalization of various meson masses to the lowest Matsubara frequency removes all thermal dependence of the bound mesons and estimates the individual dissolving temperatures. It has been found that the various mesonic states have different dissolving temperatures and baryon chemical potentials, i.e., they survive the *typically averaged* QCD phase boundary, defined by the QCD critical temperatures with varying baryon chemical potentials.

We have studied the thermal behavior of meson masses in the large-N_c limit. At low temperatures, we find that the meson masses are stable and noninteracting. With increasing temperature, they keep the mass gap between the different meson channels. At high T, this gap disappears and the masses become T independent. The scalar meson masses are T independent at large N_c and high T (except π and σ). For the pseudoscalar meson masses, the large-N_c limit unifies the T dependence of all states in a universal bundle. The same is also observed for axial and axial-vector meson masses in the large-N_c limit.

ACKNOWLEDGMENTS

This research has been supported by the World Laboratory for Cosmology and Particle Physics (WLCAPP), Cairo, Egypt, http://wlcapp.net/. The authors are very grateful to the anonymous referee for her/his constructive suggestions. A.T. would like to thank Dirk H. Rischke and Denis Parganlija for fruitful discussions careful reviewing of the manuscript.

[1] M. Gell-Mann and M. Levy, Nuovo Cimento **16**, 705 (1960).
[2] C. Amsler and N. A. Tornqvist, Phys. Rep. **389**, 61 (2004).
[3] E. Klempt and A. Zaitsev, Phys. Rep. **454**, 1 (2007).
[4] C. Vafa and E. Witten, Nucl. Phys. B **234**, 173 (1984); L. Giusti and S. Necco, J. High Energy Phys. 04 (2007) 090.
[5] A. M. Polyakov, Phys. Lett. B **72**, 477 (1978).
[6] L. Susskind, Phys. Rev. D **20**, 2610 (1979).
[7] B. Svetitsky and L. G. Yaffe, Nucl. Phys. B **210**, 423 (1982).
[8] B. Svetitsky, Phys. Rep. **132**, 1 (1986).
[9] J. T. Lenaghan and D. H. Rischke, J. Phys. G **26**, 431 (2000).
[10] N. Petropoulos, J. Phys. G **25**, 2225 (1999).
[11] M. Levy, Nuovo Cimento **52**, 23 (1967).
[12] B. Hu, Phys. Rev. D **9**, 1825 (1974).
[13] J. Schechter and M. Singer, Phys. Rev. D **12**, 2781 (1975).
[14] H. B. Geddes, Phys. Rev. D **21**, 278 (1980).
[15] B.-J. Schaefer and M. Wagner, Nucl. Phys. **62**, 381 (2009).
[16] H. Mao, J. Jin, and M. Huang, J. Phys. G **37**, 035001 (2010).
[17] J. Wambach, B.-J. Schaefer, and M. Wagner, Acta Phys. Pol. Suppl. **3**, 691 (2010).
[18] A. Tawfik, N. Magdy, and A. Diab, Phys. Rev. C **89**, 055210 (2014).
[19] A. N. Tawfik and N. Magdy, J. Phys. G **42**, 015004 (2015).
[20] A. N. Tawfik and N. Magdy, Phys. Rev. C **90**, 015204 (2014).
[21] B.-J. Schaefer, M. Wagner, and J. Wambach, PoS(**CPOD 2009**) 017 (2009).
[22] B.-J. Schaefer and M. Wagner, Phys. Rev. D **85**, 034027 (2012).
[23] B.-J. Schaefer and M. Wagner, Phys. Rev. D **79**, 014018 (2009).
[24] U. S. Gupta and V. K. Tiwari, Phys. Rev. D **81**, 054019 (2010).
[25] V. K. Tiwari, Phys. Rev. D **88**, 074017 (2013).
[26] T. Xia, L. He, and P. Zhuang, Phys. Rev. D **88**, 056013 (2013).
[27] P. Costa, M. C. Ruivo, C. A. de Sousa, H. Hansen, and W. M. Alberico, Phys. Rev. D **79**, 116003 (2009); P. Costa, M. C. Ruivo, C. A. de Sousa, and Yu. L. Kalinovsky, *ibid.* **71**, 116002 (2005); **70**, 116013 (2004).
[28] S. Borsanyi *et al.*, J. High Energy Phys. 0906 (2009) 088.
[29] S. Borsanyi *et al.*, J. High Energy Phys. 09 (2010) 073.
[30] A. Bazavov *et al.* (HotQCD Collaboration), Phys. Rev. D **85**, 054503 (2012).
[31] S. Aoki *et al.* (PACS-CS Collaboration), Phys. Rev. D **81**, 074503 (2010).
[32] S. Durr *et al.*, Science **322**, 1224 (2008).
[33] J. Beringer *et al.* (Particle Data Group), Phys. Rev. D **86**, 010001 (2012).
[34] B.-J. Schaefer, M. Wagner, and J. Wambach, Phys. Rev. D **81**, 074013 (2010).
[35] R. Stiele, E. S. Fraga, and J. Schaffner-Bielich, Phys. Lett. B **729**, 72 (2014).
[36] D. Parganlija, F. Giacosa, and D. H. Rischke, Phys. Rev. D **82**, 054024 (2010).

[37] S. Gallas, F. Giacosa, and D. H. Rischke, Phys. Rev. D **82**, 014004 (2010).
[38] D. Parganlija, P. Kovacs, G. Wolf, F. Giacosa, and D. H. Rischke, Phys. Rev. D **87**, 014011 (2013).
[39] P. Kovacs, G. Wolf, F. Giacosa, and D. Parganlija, Europhys. J. **13**, 02006 (2011).
[40] D. Parganlija, P. Kovacs, G. Wolf, F. Giacosa, and D. H. Rischke, AIP Conf. Proc. **1520**, 226 (2013).
[41] B.-J. Schaefer, J. M. Pawlowski, and J. Wambach, Phys. Rev. D **76**, 074023 (2007).
[42] L. M. Haas, R. Stiele, J. Braun, J. M. Pawlowski, and J. Schaffner-Bielich, Phys. Rev. D **87**, 076004 (2013).
[43] A. Tawfik and N. Magdy (unpublished).
[44] S. Struber and D. H. Rischke, Phys. Rev. D **77**, 085004 (2008).
[45] J. T. Lenaghan, D. H. Rischke, and J. Schaffner-Bielich, Phys. Rev. D **62**, 085008 (2000).
[46] D. Parganlija, F. Giacosa, and D. H. Rischke, AIP Conf. Proc. **1030**, 160 (2008).
[47] D. Parganlija, F. Giacosa, and D. H. Rischke, PoS(**CONFINEMENT 8**) 070 (2008).
[48] V. Koch, Int. J. Mod. Phys. E **6**, 203 (1997).
[49] S. Gasiorowicz and D. A. Geffen, Rev. Mod. Phys. **41**, 531 (1969).
[50] P. Ko and S. Rudaz, Phys. Rev. D **50**, 6877 (1994).
[51] J. Boguta, Phys. Lett. B **120**, 34 (1983); O. Kaymakcalan and J. Schechter, Phys. Rev. D **31**, 1109 (1985); R. D. Pisarski, talk at workshop on Finite Temperature QCD and Quark-Gluon Transport Theory, 18–26 April 1994, Wuhan, China (unpublished).
[52] P. Kovacs and G. Wolf, Acta Phys. Pol. Suppl. **6**, 853 (2013).
[53] C. Rosenzweig, J. Schechter, and C. G. Trahern, Phys. Rev. D **21**, 3388 (1980).
[54] A. H. Fariborz, R. Jora, and J. Schechter, Phys. Rev. D **77**, 094004 (2008).
[55] S. Weinberg, Phys. Rev. D **11**, 3583 (1975).
[56] D. H. Rischke and D. Parganlija (private communication).
[57] V. I. Borodulin, R. N. Rogalev, and S. R. Slabospitsky, CORE: COmpendium of RElations: Version 2.1, arXiv:hep-ph/9507456.
[58] P. Kovacs and Z. Szep, Phys. Rev. D **75**, 025015 (2007).
[59] K. Fukushima, Phys. Lett. B **591**, 277 (2004).
[60] C. Ratti, M. A. Thaler, and W. Weise, Phys. Rev. D **73**, 014019 (2006).
[61] S. Rossner, C. Ratti, and W. Weise, Phys. Rev. D **75**, 034007 (2007).
[62] K. Fukushima, Phys. Rev. D **77**, 114028 (2008).
[63] B.-J. Schaefer and J. Wambach, Phys. Rev. D **75**, 085015 (2007).
[64] O. Scavenius, A. Mocsy, I. N. Mishustin, and D. H. Rischke, Phys. Rev. C **64**, 045202 (2001).
[65] J. I. Kapusta and C. Gale, *Finite-Temperature Field Theory: Principles and Applications* (Cambridge University Press, Cambridge, 2006).
[66] A. Bazavov (HotQCD Collaboration) PoS(**LATTICE 2011**) 182 (2011).
[67] A. Tawfik, Phys. Rev. D **71**, 054502 (2005).
[68] Y. Aoki, G. Endrodi, Z. Fodor, S. D. Katz, and K. K. Szabo, Nature (London) **443**, 675 (2006).
[69] E. Laermann, Nucl. Phys. A **702**, 134 (2002).
[70] D. Parganlija, P. Kovacs, G. Wolf, F. Giacosa, and D. H. Rischke, PoS (**ConfinementX**) 117 (2012).
[71] J. Kapusta, *Finite-Temperature Field Theory* (Cambridge University Press, Cambridge, 1989).
[72] M. Wagner, Thesis, Technische Universität Darmstadt, 2008 (unpublished).
[73] E. Witten, Nucl. Phys. B **156**, 269 (1979); G. Veneziano, *ibid.* **159**, 213 (1979).
[74] W. Florkowski and B. L. Friman, Z. Phys. A **347**, 271 (1994).
[75] K. Dusling, C. Ratti, and I. Zahed, Phys. Rev. D **79**, 034027 (2009).
[76] A. Tawfik, Soryushiron Kenkyu **114**, B48 (2006).
[77] G. 't Hooft, Nucl. Phys. **75**, 461 (1974); E. Witten, Nucl. Phys. B **160**, 57 (1979).
[78] A. Heinz, F. Giacosa, and D. H. Rischke, Phys. Rev. D **85**, 056005 (2012).
[79] F. Giacosa, arXiv:1106.0523.
[80] L. D. McLerran and R. D. Pisarski, Nucl. Phys. A **796**, 83 (2007); Y. Hidaka, L. D. McLerran, and R. D. Pisarski, *ibid.* **808**, 117 (2008).
[81] J. D. Walecka, Ann. Phys. (NY) **83**, 491 (1974); B. D. Serot and J. D. Walecka, Adv. Nucl. Phys. **16**, 1 (1986); Int. J. Mod. Phys. E **6**, 515 (1997).
[82] L. Bonanno and F. Giacosa, Nucl. Phys. A **859**, 49 (2011).